An Electromechanical Coupled Model of the Probe of a Scanning Fiber Imaging System

Abhijith Rajiv

A thesis submitted in partial fulfillment of the requirements for the degree of

Master of Science in Mechanical Engineering

University of Washington
2016

Committee:

Per Reinhall, Chair

Eric Seibel

Jonathan T.C. Liu

Program Authorized to Offer Degree:
Department of Mechanical Engineering

University of Washington

Abstract

An Electromechanical Coupled Model of the Probe of a Scanning Fiber Imaging System

Abhijith Rajiv

Chair of the Supervisory Committee:

Prof. Per Reinhall

Department of Mechanical Engineering

A higher fidelity electromechanical model of the piezoelectric actuator coupled to the optical fiber in a scanning fiber imaging system is developed and solved using finite element software and validated to predict certain system characteristics with good accuracy. Experimental data collected is also used to study the effect of some design and control choices in the transition between linear to non-linear operating regimes for these scanning systems. Alternative reduced order non-linear models are developed to handle predicting system characteristics for such non-linear scanners. A model based design approach is also presented for an iterative design-build-test approach to development of this technology. The capabilities of the models in evaluating effectiveness of unconventional fiber scanner designs is also explored.

Acknowledgments

The task of completing this study successfully has been possible only with the support and guidance of a number of people.

I am thankful to my advisor Professor Per Reinhall, for introducing me to this exciting technology and giving me an opportunity to learn and contribute to its development. I am grateful, for his wisdom has helped me overcome unexpected challenges encountered throughout this study. I am also thankful to my advisor Prof. Eric Seibel for providing me the opportunity to work on this system and offering his valuable time and feedback and also lab resources towards completion of this project. I am also thankful to my advisor Prof. Jonathan T.C. Liu for his valuable feedback and constructive criticism that helped me look at this project from different perspectives and get more meaning out of it.

I am thankful to my colleagues at the Human Photonics Lab here at the University of Washington, especially lab engineers Catherine Olivo who fabricated all the scanner systems I used for the experiments, Richard Johnston for his insights into understanding this system and Matt Carson for offering me his technical expertise in solving challenges. I would also like to thank all my family and friends for their whole-hearted support and encouragement. I would also like to appreciate the financial support I received from the Department of Mechanical Engineering in the form of teaching and research assistantships.

Table of Contents

List of Figures

List of Tables

1. INTRODUCTION

Conventional imaging and display systems consist of a grid of light sensitive sensors that capture light reflected off of the area being imaged. In such systems the FOV and resolution of the image depends on the size of this sensor and in modern endoscopy, a wide field of view and resolution are highly desirable in order to increase chances of detecting features that could help in diagnosis of conditions. These requirements put a limit on how small the endoscope probe can be made which can limit the usage of such probes in harder to reach parts of the human body. A new and versatile technology has emerged in this field called a scanning fiber endoscope, which enables high quality video imaging at the same time keeping the probe sizes as low as 1.2 mm in diameter [1]. In comparison existing endoscopy technologies have probes that only go up to as small as 6.4 mm in diameter [2].

The Scanning Fiber Endoscope (SFE) technology performs active scanning of laser light vibrating a single mode optical fiber near its mechanical resonance frequency. This optical fiber is held by a small piezoelectric actuator with a certain length of the optical fiber held as a cantilever on the free end of this tube actuator. Drive signals causes the actuator to vibrate, which moves the base of the cantilevered fiber. Being close to the resonance frequency allows $\pm$ 4 mm fiber tip deflections and around 100° wide FOV. The light emitted by the fiber then hits the objects in the area being scanned and is reflected back. The bundle of collection fibers collects this light and returns it the back end where hardware and software are used to process the light information and recreate the image of the area being scanned.

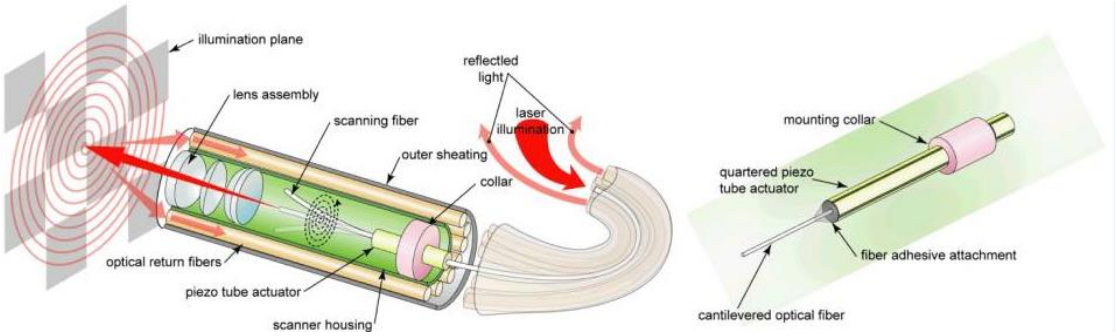

Figure 1: Functional diagram of the SFE with the scanning fiber moving in a spiral pattern (left) and a magnified view of the main mechanical components (right). Image from [1]

Although several studies have been done and published on the fiber scanner system, this study focuses on some unique approaches that have not been done before. The first feature is to have a model that can predict variations in system characteristics based on changes in the geometrical design of the mechanical parts of the scanner. That is to have one model with all the main mechanical parts of the scanner assembly 'coupled' together, such that if the design of one of these parts is varied, a qualitative or quantitative estimation of can be made of its effect on the dynamics of the scanner system as a whole. The second feature is to have a model in which an input can be applied to the piezoelectric actuator as an electric voltage and be able to estimate the mechanical properties of the system. Previous studies developed and used models where an input displacement is applied on the end of the piezoelectric actuator that holds the fiber, which is representative of the deflection it would have had if a drive voltage was applied to it. Such models ignore the dynamics added due to piezoelectric effects.

The third feature is to develop model based design processes for coming up with system designs that can achieve desired system performance characters. Previous studies have either used a lumped parameter model estimated using experimental data or a system identification approach to estimate transfer functions from experimental data. In all such approaches, the system needs to be built first and then experiments need to be done on it in order to see how that particular design behaves dynamically. But this study aims to develop a model that can predict system characteristics and thus estimate transfer functions of that particular design before the scanner is even built. This new scanning

fiber imaging technology has now moved from the initial state of proving functionality and is heading towards the optimization phase of technology development. Thus a better understanding has to be had of every component of this scanner system and how each design and fabrication choice can affect the dynamics of the system once its built. Also new fiber designs and designs of the other parts of the system are being actively researched upon in order to improve or optimize performance. The combination of the first and the third features of this study makes the models developed and data collected, a valuable tool in such endeavors.

2. FIBER SCANNER SYSTEM

As the idea behind this study is to develop a dynamic model of the fiber scanner system and also to validate it, the scope of the study is limited to a subsystem of the actual fiber scanner probe that can be set up to collect validation data. This section divides the fiber scanner system under study into the following components and goes into detail about each component geometry, material and how the component was modeled and describes differences with the same component in the experimental set up. The exact material properties are given in Appendix A.

- Piezo-tube holder (holder)
- Ceramic Collar
- Piezoelectric actuator tube (piezo-tube)
- Joint between the piezo-tube and the optical fiber (CA joint)
- Optical fiber (fiber)

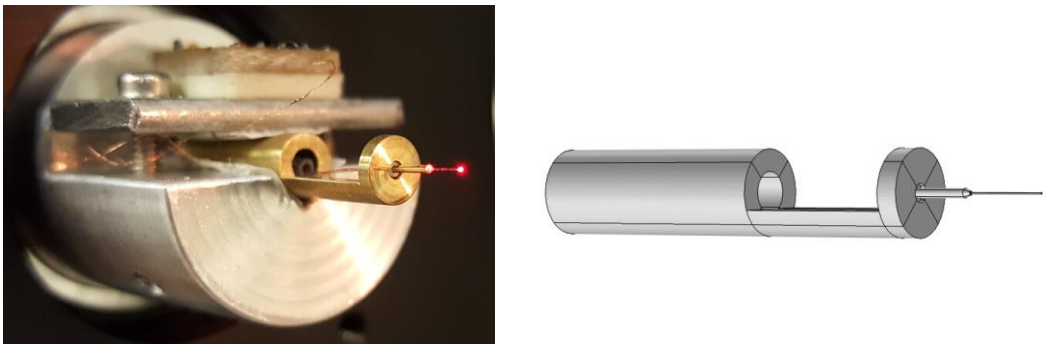

Figure 2: Fiber scanner setup used for validation experiments (left) and fiber scanner model CAD geometry (right)

2.1. Piezo-tube holder (Holder)

The experimental set up involves a piezo-tube holder, which is different in design from the actual housing that holds the piezo-tube in a production scanner. This is necessary to provide better access to the components of the fiber scanner for executing the procedure of the experiment and for data collection. This modified design piezo tube holder enables this study to:

- Estimate actual fiber tip deflection

- Cleave the fiber while it is a part of the scanner system, in order to have every variant as similar as possible to the baseline, except for the parameter being compared

Thus it is to be noted that this piezo-tube holder is not a part of the actual fiber scanner probe, but it will be included in the model being developed, so as to improve accuracy towards the validation data.

The holder is a cylindrical tube (Figure 3) that holds the ceramic mount, which in turn attaches to the piezo-tube. The fiber and the wires to the terminals on the piezo-tube are routed through the tube through the whole on the backside. The tube is clamped on to the experimental setup. The holder is made of brass which generally exhibits linear elastic material behavior [3].

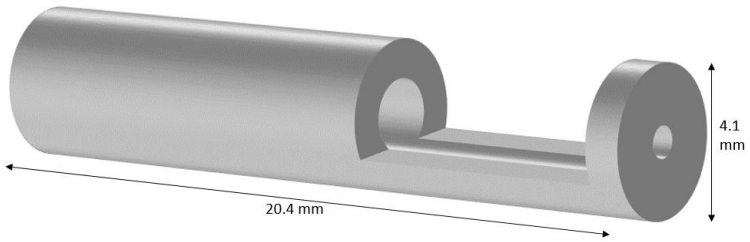

Figure 3: CAD diagram of the Piezo-tube holder

In previous works it was assumed that the dynamics of the holder does not contribute significantly to the dynamics of the scanner as a whole. Thus this study first started off without the holder being modeled. But it is later added in due to the following reasons.

- During experiments, it was noticed that the holder had a resonance close to the resonance of the fiber being tested.
- As the experimental setup used to obtain validation data included the holder, it is included in the model too to improve accuracy without too much overhead.
- The geometry of the rest of the components is axisymmetric by design, whereas the geometry of the holder is not. This is significant as this study involves a 3D model and it is later seen that asymmetry in the geometry can affect the frequency response and hence the dynamics of the scanner system as a whole (Section 8.1**Error! Reference source not found.**).

The variant of brass is assumed to be UNS C36000 and material properties are obtained from [4].

2.2. Ceramic Collar

To provide electrical insulation between the terminals of the piezo-tube and the brass holder, the piezo-tube is first attached to a ceramic collar before being mounted on the holder. The collar and piezo-tube and also the collar and holder are held together using cyanoacrylate glue (instant adhesive). These boundaries are assumed to be rigid for the model and the dynamics of the boundary itself is not modeled. The ceramic collar (Figure 4) itself is a cylindrical tube, with an inner diameter almost the same as the outer diameter of the piezo-tube. The collar is of an alumina type ceramic. The exact material properties of the ceramic was not readily available. For the model, it is assumed to be a 96% Al_2O_3 ceramic and material properties are obtained from [5].

2.3. Piezoelectric Actuator Tube (Piezo-tube)

The actuator that drives the scanning system is a piezoelectric ceramic tube (Figure 4). The material of the tube in specific is PZT-5A and material properties are obtained from the COMSOL material library. This material specifically is classified as a ferroelectric material, which falls under a sub-category of piezoelectric ceramics [6]. The tube is manufactured by Nagamine Manufacturing Co. Ltd. A double layer of first Nickel and then Gold, is applied on the stock piezo-tube to make it curved surface conducting. Ridges are then cut on this coated surfaces along the length of the tube, such that the entire curved surface area of the tube is divided into four electrically conducting surfaces. Copper wires are soldered onto the fixed end of the piezo-tube, one for each surface, effectively making each of these surfaces a terminal where input drive voltage can be applied. The optical fiber is also drawn through the piezo-tube to the illumination source. The free end of the piezo-tube which hold the fiber is also wound with Kevlar strings for additional strength to prevent cracking during operation. The conductive coating, ridges, copper wires and the Kevlar winding are excluded from the model for simplicity.

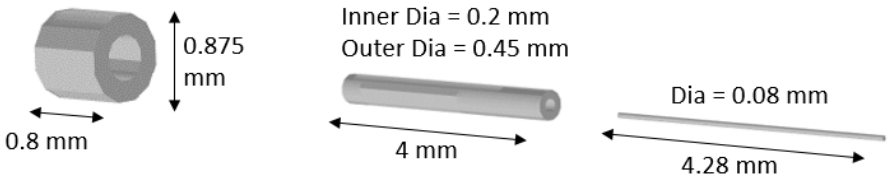

Figure 4: The Collar, Piezo-tube and Fiber

2.4. Optical Fiber (Fiber)

The optical fiber, which is the main imaging component is a very long strand of fiber made of silica glass. It was purchased from StockerYale (now named ProPhotonix). It is a single cut-off single-mode fiber with a cladding diameter of 80 microns. The material properties are obtained from the COMSOL material library. The actual fiber in the experimental setup is long and extends from the fiber tip extending out of the piezo tube to the illumination source that is used for imaging. The part of the fiber (Figure 4) which is in the piezo-tube and ahead of it, is the main component that affects the mechanical dynamics of the scanning probe. The fiber inside the piezo-tube is held in place using two droplets of Silicone rubber elastomer close to each end of the piezo-tube (Figure 5). It is assumed that the droplet on the distal end of the piezo-tube is rigid enough to force the deflection of that part of the fiber and piezo-tube to be the same. This assumption that the silicone droplet acts as a rigid boundary between the fiber and the piezo-tube allows exclusion of the rest of the fiber on the proximal side, behind the droplet from being modeled. The silicone droplets are assumed to not add anything more to the dynamics of the scanner and are thus not modeled.

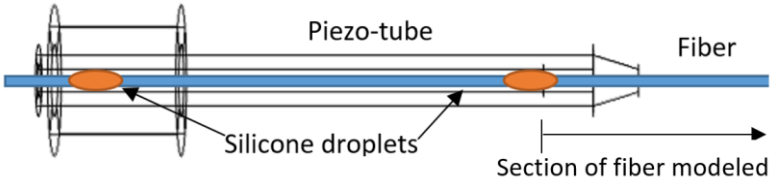

Figure 5: Positioning of fiber inside the piezo-tube

2.5. Joint between the piezo-tube and the optical fiber (CA joint)

The fiber and the piezo-tube are coupled together at the distal end. This joint is usually made using epoxy [7]. But as the scanner used in this study is more of a test prototype scanner which may have to go through multiple disassembly and reassembly, a

cyanoacrylate (CA) glue is used instead. This offers the advantage that even cured CA glue can be removed using acetone, without damaging the bonding surfaces. This study focuses more on modeling the mechanics of each component with respect to its elastic behavior and geometry. Thus even though the material properties of epoxies and CA are different, as both epoxies and CA are viscoelastic materials, this change does not affect the study. For a scanner using epoxy, the material parameter constants in the model would just need to be changed. Thus for the rest of this work, everything discussed about the CA glue is also applicable correspondingly to an epoxy joint.

Modeling the geometry of this joint is also challenging as the transition of CA from a liquid state to a cured solid state is not well controlled [7]. After the fiber is positioned inside the piezo tube, based on the design geometry, cyanoacrylate is applied as liquid to the free end of the piezo tube between the piezo-tube and the fiber. Due to capillary action CA in its liquid state also flows into the piezo tube and fills up the space between the fiber and the piezo tube to some extent, before it sets into a solid state. A general shape of a CA joint resulting from these processes is shown in Figure 6. This is the geometry of the joint used in the model described in the rest of the study. The material properties of the exact brand of CA glue used is not available. Density values are obtained from similar products from a different brand [8]. Similarly the ASTM D2240 hardness was also available from [8]. As other studies [9] have shown that the ASTM D2240 hardness of an elastomer is correlated to the Young's modulus, the Young's Modulus and Poisson's ratio of an epoxy with similar hardness values were used for modeling of the CA joint. It is important to note that even though CA glue is also used to join other components together as mentioned earlier, only the glue between the piezo-tube and optical fiber is modeled as the rest of the component interfaces are assumed to be just rigid connections.

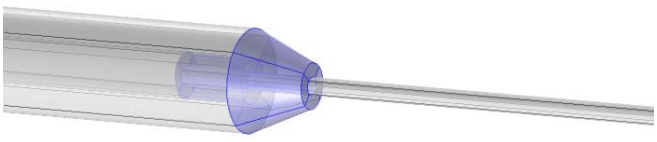

Figure 6: Joint (blue) between piezo-tube and fiber

3. Coupled Model Development

3.1. Material Models

The components described in Section 2 can be classified into the following based on their mechanical behavior to stress and strain.

- Linear elastic material (holder, collar, fiber)
- Viscoelastic material (CA joint)
- Piezoelectric material (piezo-tube)

For the sake of simplicity, this study focuses on the linear elastic and piezoelectric material types. Viscoelastic materials basically show both viscous and elastic material behavior when undergoing deformations. Thus in addition to elastic behavior they also show properties like hysteresis between stress and strain and creep behavior (constant stress causes strain that increases with time). As the applications for fiber scanning systems usually involve only high frequency vibrations, the effect due to creep is considered minimal. This study chooses to model the CA joint as a linear elastic material. The energy loss due to hysteresis is taken into account as an isotropic loss factor for the whole material medium, as explained in later sections.

3.1.1. Linear Elastic Material Model

For linear elastic materials, the constitutive equations are given by, Hooke's law [10]:

$$\sigma = C\varepsilon \tag{3.1}$$

Here σ, C and ε are the stress, elastic strain and elasticity tensors respectively. Assuming isotropic material symmetry, the stress and elastic strain tensors can be reduced to 3x3 matrices. Similarly, the elasticity tensor reduces to a 6x6 matrix with the Young's modulus and Poisson's ratio defining it.

A viscoelastic material's response is specifically affected by a complex valued modulus. The real part represents the storage modulus which controls the elastic response and the imaginary part represents the loss modulus which represents the viscous component. Storage modulus acts as a good approximation of the Young's modulus for an epoxy [11].

As explained in Section 2.5, this was used to approximate the Young's modulus of the linear elastic material model for the CA joint.

3.1.2. Piezoelectric Material Model

Piezoelectric materials are materials that can convert mechanical energy into electrical energy through the direct piezoelectric effect and vice versa through the inverse piezoelectric effect. This effect in most materials is due to an inherent asymmetry in the crystal structure [6]. In addition to exhibiting piezoelectric material behavior, the material used in the piezo-tube PZT-5A, also exhibits properties of ferroelectricity. This is a property which is defined by a spontaneous electric polarization which sustains in the material even after the polarizing field is removed and this polarization (P) can then be reversed by application of another external electric field (E) [12]. Cyclic polarization and depolarization results in a hysteresis loop as shown in Figure 7. The piezo-tubes used in production fiber scanners and the experiments done as a part of this study are polarized during assembly of the probe through a process known as poling. Even though this material can show this non-linear hysteretic behavior, the normal operation ranges for the fiber scanner is well within the point C and C' in Figure 7. Here the point P_s refers to the remnant polarization left in the material due to the initial poling process. During a drive cycle, the piezo-tube is driven in the operating region on the curve between the points P_s and C or on the corresponding points in the bottom negative quadrants. This region of the curve is mostly linear and thus a linear piezoelectric material model can be used to model the dynamics. A slight modification is made to take remnant polarization into account.

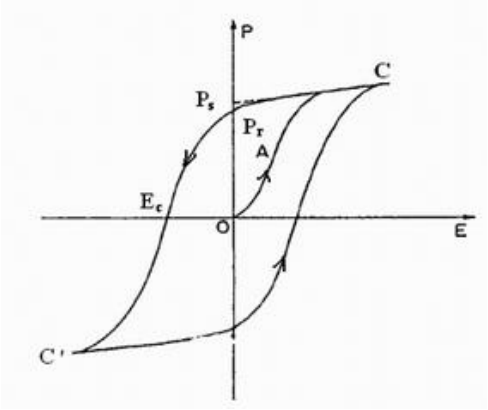

Figure 7: P-E hysteresis loop for a typical ferroelectric material [13]

The piezoelectric material constitutive equations represented in 'stress-charge' form is given by:

$$\sigma = C\varepsilon - e^T E \tag{3.2}$$
$$D = e\varepsilon + \epsilon_S E + D_r$$

Here e represents the coupling matrix, E represents electric field, D, D_r represent electric displacement and electric displacement due to remnant polarization and ϵ_S represent material permittivity respectively.

During the poling process, electric fields are applied such that the piezo-tube is polarized radially. This is to maximize deflection during a drive cycle. This introduces an anisotropy in the material properties. Thus the material property matrices need to be transformed from a Cartesian coordinate frame the material property values are obtained from to the frame corresponding to the direction of poling. This is done in two steps, first to convert from Cartesian to Cylindrical coordinate system and then a rotation to align to a radially outward remnant polarization. The rotation matrix for this transformation is given by,

$$\begin{bmatrix} \hat{r} \\ \hat{\theta} \\ \hat{z} \end{bmatrix} = \begin{bmatrix} cos\theta & sin\theta & 0 \\ -sin\theta & cos\theta & 0 \\ 0 & 0 & 1 \end{bmatrix} \begin{bmatrix} \hat{x} \\ \hat{y} \\ \hat{z} \end{bmatrix} \; where\; \theta = \tan^{-1}\left(\frac{y}{x}\right) \tag{3.3}$$

3.2. Finite Element Model Formulation

The assembling of material model equations, finite element meshing and formulation and solution are done using COMSOL software. The software offered advanced features like availability of a piezoelectric material model, integrated material library, in-built

parametric sweep feature, second Piola-Kirchhoff stress tensor and Green-Lagrange strain tensor formulations to model geometric non-linearity and solvers with varying fidelity for time and frequency domain analysis [14].

3.2.1. Meshing

Although COMSOL software can automatically mesh geometry using a tetrahedral mesh, a custom mesh was generated for all components. This was done in order to avoid introducing any geometric asymmetry. An exception is the holder, which was meshed using the default COMSOL meshing algorithm as the holder is asymmetric by design. Thus the holder is made of tetrahedral meshing elements which are not necessarily symmetric. The custom mesh for the rest of the components are made by generating a triangular mesh for an axial cross-section of each component and then sweeping this around the longitudinal axis. This generates an axisymmetric 3D mesh made of prism, tetrahedral and pyramid elements such that all the external surfaces are the quadrilateral bases of the prism element. An illustration of each element type is provided in Figure 8.

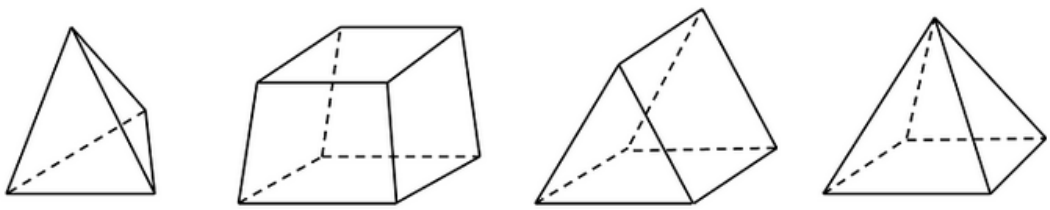

Figure 8: 3D mesh element types: Tetrahedral, Brick, Prism, Pyramid (left to right) [15]

At the surfaces where the prism and pyramid elements' base interface with the tetrahedral elements, the quadrilateral mesh surface of the base is split into two triangular surfaces. It was seen during the study that if asymmetry is introduced during meshing, the simulation results would more closely resemble that of system with asymmetric geometry.

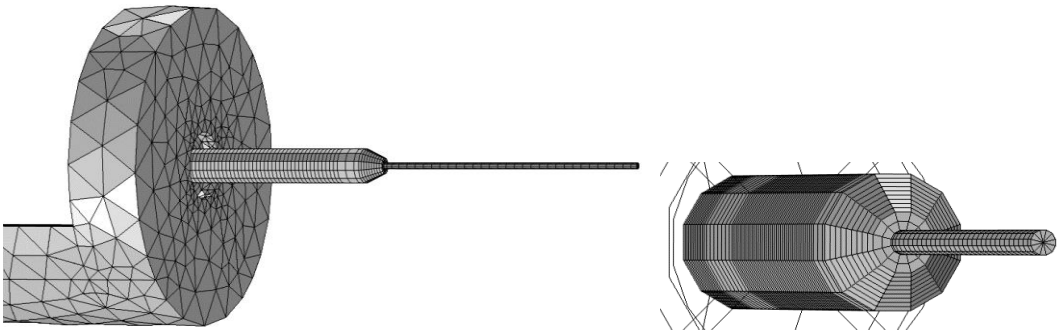

Figure 9: Meshed Geometry, zoomed in on the fiber on the right

Mesh refinement analysis was run based on the study type to optimize tradeoff between computational speed and accuracy. For example, if a solver that computes eigenvalues of the system is being run then mesh was refined until the eigenvalues converged. Figure 10 below shows convergence of the computed frequency response of the system as mesh on the fiber is made finer. The quality of a mesh element, defined as the ratio of the shortest to the longest side is controlled to avoid having elements that are too skewed. A mesh quality greater than 0.1 is considered acceptable [16].

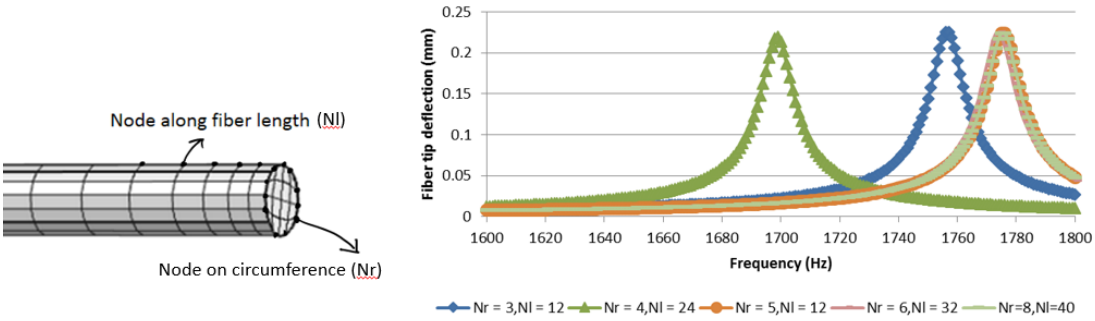

Figure 10: Computed frequency response converges as mesh on the fiber is made finer

3.2.2. Boundary Conditions

For most of the simulations, there are two boundary conditions, unless specified otherwise.

- Constraint on the holder as it is clamped on one end. The displacement on the top and bottom surface on the part of the holder in the clamp is considered 0.
- Voltage input on the piezo tube that drives the system. As mentioned in Section 2.3, the piezo-tube has four separate terminals on the outer surface. In the model,

due to perfect symmetry, only one pair of terminals from among the total four terminals need to be excited, to get the fiber to scan in a straight line. On the actual system, due to imperfections in the material and the manufacturing processes, there is some asymmetry. Due to this asymmetry the principle axes of the piezo-tube and the fiber need not be aligned. Thus to get the fiber to scan in one direction, input voltages need to be applied on both the orthogonal axes pairs on the piezo-tube [7].

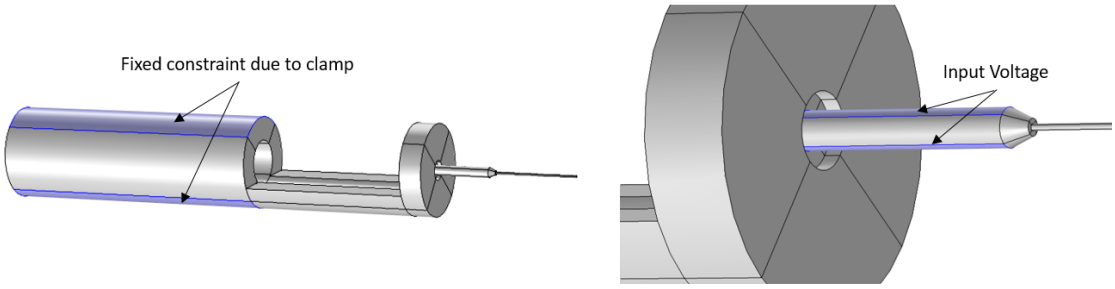

Figure 11: Boundary conditions on the model. Input voltage is set to be on the pair of terminals highlighted in the figure or the other pair of terminals

3.2.3. Solvers

Once the geometry, physics and boundary and initial conditions are set up, a solver is chosen based on whether solutions are needed in time or frequency domain and based on what variables of the system need to be solved for. Regardless of the solver type, they all start by assembling all the physics equations and constraints into a form that can be discretized and solved numerically. The physics equations include equation of motion for mesh nodes in all components (3.4) and electrostatics equations for mesh nodes in the piezo-tube (3.5).

$$\rho \frac{\partial^2 u}{\partial t^2} = \nabla . \sigma + F_v \tag{3.4}$$

$$E = -\nabla \mathrm{V} \tag{3.5}$$

Here u is the displacement vector, ρ is density, σ is the first Piola-Kirchoff stress tensor, F_v is force vector per unit volume, E is the electric field vector and V is the electric potential. The displacement vector is related to the Green-Lagrange strain tensor ε as,

$$\varepsilon_{ij} = \frac{1}{2}\left(\frac{\partial u_i}{\partial x_j} + \frac{\partial u_j}{\partial x_i} + \frac{\partial u_k}{\partial x_i}\frac{\partial u_k}{\partial x_j}\right) \tag{3.6}$$

The strain tensor and stress tensor are related by Equations (3.1) and (3.2). The stress tensor is then related to internal and external force vectors. In the particular case of piezo-tube Equation (3.2) also introduces the electric field variable, which is then related to the electric potential by Equation (3.5). Thus both the equations of mechanics and equations of electrostatics are fully coupled. Next these equations applied to the appropriate nodes are discretized in space, based on the mesh. Now boundary conditions are applied and the remaining unknown variables, which are the degrees of freedom of the system are identified. The equations are then solved to compute the unknown variables. If the equations are fully coupled and displacements and voltages are affect each other, then the equations are solved iteratively from a starting initial guess for the solution. The iterations are continued until the estimate for relative error is within tolerance. Relative error is estimated by 'deferred correction' [17]. This section will now go through the different solvers used for this study.

- The eigenvalue solver is used to compute natural and damped frequencies and also to tune the damping ratio for each mode. The results of this solver is also used to setup a reduced order modal solver to compute the frequency response of the system. This solver converts equations (3.4) and (3.5) to Laplace domain by taking a Laplace transform of every time dependent function and time based operator. The external inputs are set to zero as this is an eigenvalue solver. Then as usual, a homogenous solution of exponential form is assumed and substituted in the place of u resulting in a set of equations of a quadratic eigenvalue system,

  $$\nabla.\Sigma(\mathrm{U}) = \rho\lambda^2 U \tag{3.7}$$

  Here λ denotes the eigenvalues, U is an eigenvector and $\Sigma(\mathrm{U})$ is the stress vector as a linearized function of displacement. The solver then uses the ARPACK routine [17], which estimates a requested number of eigenvalues in a requested search region by solving this system of equations. This solving of linear equations is done using the Multifrontal Massively Parallel Sparse Direct (MUMPS) solver [18] inbuilt in COMSOL.

- Transient/time domain solver is used to compute the transient response of the system to the inputs. It basically uses the Generalized Alpha method for discretizing terms containing functions or operators of time in Equation (3.4). The resulting set of linear equations after temporal and spatial discretization and coupling between physics is again solved using the MUMPS solver.
- Frequency domain solver is used to compute the frequency response of the system. This solver works similar to the eigenvalue solver by converting Equations (3.4) and (3.5) in Laplace/frequency domain, but also considers the voltage inputs to be harmonic functions. That is,

$$V = V_{in} e^{i\omega t} \tag{3.8}$$

  Here V_{in} is the amplitude of the harmonic excitation input. The resulting equations are linearized and solved using the linear MUMPS solver.
- Modal solver is used to obtain frequency response of the system albeit with some assumptions, which speeds up the computation drastically. While the frequency domain solver actually solves the system of equations in frequency domain, the modal solver uses the eigenvalues and eigenvectors of the system to come up with a reduced order approximation for the unknown variables to be computed. This approximation is basically a linear combination of a requested number of eigenvectors and their unknown coefficients. This method also assumes that all appearing Dirchlet boundary conditions are homogenous and that all the dominant eigenmodes have been included in the solution approximation. The solver then solves for these unknown coefficients using the MUMPS solver.

3.2.4. Damping

One of the biggest challenges when modeling structural mechanics is to estimate the damping in the system. Presence of multiple components and electro-mechanical coupling in the piezo-tube, makes this even more complicated. This study uses a set of tuning data from experiments to tune the damping in the model required to accurately simulate the system. Damping is added to every component using isotropic loss factors in

every constitutive matrix. That is, the modulus of the linear elastic material is represented in complex plane as,

$$C_{eq} = (1 + i\eta)C \tag{3.9}$$

Here η is the isotropic loss factor and i is the imaginary unit $\sqrt{-1}$ in the case of a linear elastic materials stiffness matrix. This form of energy dissipation is representative of the energy lost from the system on each cycle of harmonic oscillation. Thus this form of damping is not a part of the time domain equations.

In addition to structural damping, the piezo-tube also has dielectric losses in its internal electric field and coupling losses during the conversion of electrical to mechanical energy and vice versa. For the sake of simplicity, coupling losses are accounted for by adding the corresponding losses to the losses in structural deflections which is done by adjusting the isotropic loss factor. The dielectric losses are obtained from [19] and are assumed to be constant with respect to frequency and input excitation voltage. Nominal values are used for the structural damping in the holder and the collar. Optical fibers are known to have comparatively very low loss factors. Hence a nominal value of much smaller magnitude is used for the optical fiber. The loss factor values for the piezo-tube and the cyanoacrylate are tuned using the tuning data from experiments. The loss factors are varied manually until a good agreement is reached between the Q-factor from the simulations and experimental data.

3.3. Transfer Function Estimation

Model identification through parameter estimation has been used for many years to estimate transfer functions of dynamic systems from frequency response data [20]. Combining this with model based design principles, can allow estimation of transfer function for a system early during design stages, before it is even built. This transfer function can then be used for control software development and software or hardware-in-the-loop testing. In order to estimate transfer function, a transfer function order is chosen and an initial guess for all the parameters of the transfer function is assumed. Then a Prediction Error Minimization (PEM) technique is used where an attempt is made to minimize the output error from the transfer function estimated at each iteration. The

estimate for transfer function is updated at each iteration using a nonlinear least-squares search method [21]. Frequency response, both magnitude and phase, obtained from the coupled model is used as the true value about which the error is minimized. The estimation is done using MATLAB ® and the System Identification Toolbox.

4. Experiments and Data Acquisition

4.1. Drive Monitor

The scan drive monitor is a workstation developed as a part of this study for testing, and benchmarking scanner systems and for acquiring performance data for model tuning and validation and also for control software testing. The immediate and future goals that drove the design of the hardware and software include:

- Acquire data regarding the actual deflection of the fiber tip during a scan and final laser spot trajectory.
- Allow characterization of the geometry of the scanner.
- Estimate system parameters like resonance frequency, damping, principal axes orientations, etc.
- Test a scanning probe assembly and verify performance characteristics at different stages of the assembly process.
- In order to conduct a benchmark study comparing fibers at different lengths, a process to cleave the fiber in situ is also developed.

Figure 12 shows an illustration of the experimental setup.

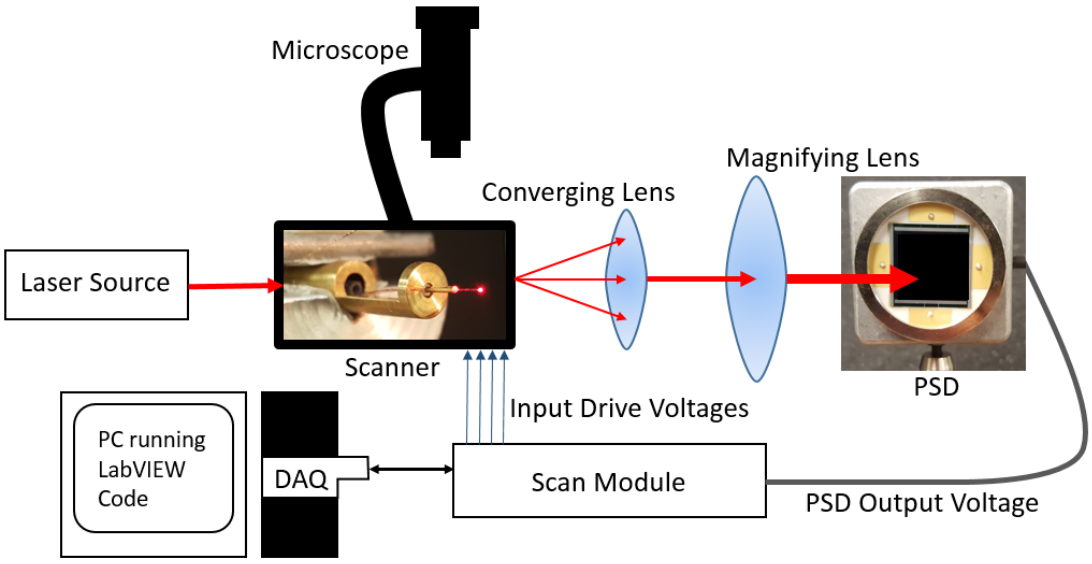

Figure 12: Illustration of the experimental setup

The microscope allows measurement of the projection of the scanner system geometry on the horizontal plane. This would be the horizontal component of the peak to peak deflection of the fiber tip. Combining information from this top view projection and the angle made by the final laser trajectory with the global coordinate system as measured through the Position Sensing Detector (PSD), allows estimation of the actual fiber tip deflection amplitude x_{act} through the equation,

$$x_{act} = \frac{x_{top}}{2\cos(\alpha)} \tag{4.1}$$

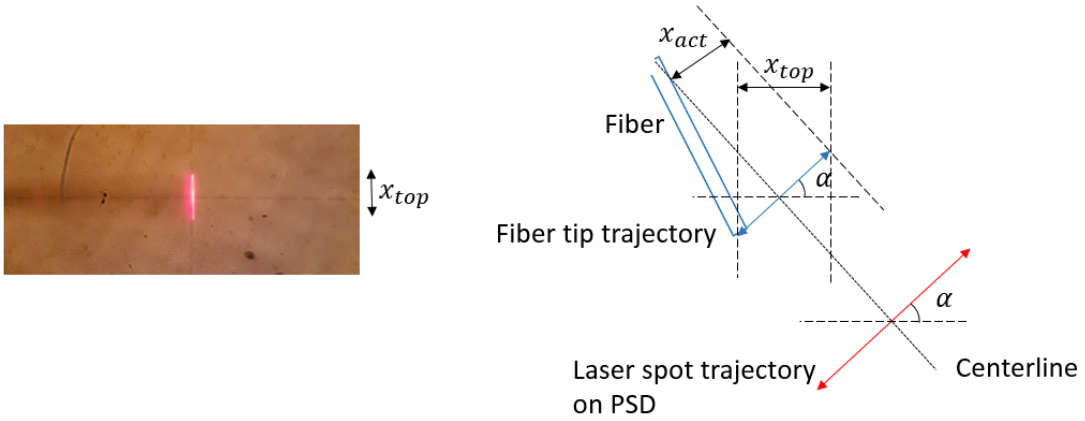

Figure 13: Top view of the fiber deflection as seen through the microscope (left), schematic of fiber tip and laser spot trajectory in 3D space (right)

The microscope also allows characterization of the geometry of the fiber tip and the geometry of the joint between the piezo-tube and the fiber.

Software was developed in LabVIEW and MATLAB with the following features:

- Generate signals to drive the piezo-tube based on user input
- Post-process the signals from the PSD for data visualization. The software would enable monitoring of the trajectory of the laser spot in 2D as it falls on the PSD's imaging sensor. Calculate α.
- Acquire frequency response of the system and with some post-processing through MATLAB also estimates resonance frequency and Q-factor.
- Allow orienting the input drive voltages along virtual electrodes to achieve whirl free excitation as demonstrated in [7].

- Characterize the variation in virtual electrodes with changes in the assembly, geometry and other features in the scanner.
- Continuously drive the scanner while the tip deflection is being observed through the microscope.

Before initializing data acquisition, the output from the PSD is calibrated such that when the scanner is not being driven the laser spot displayed in the graphical UI is set to be at origin.

4.2. Fiber Cleaving Setup

One of the main goals of this study is to be able to make relative comparisons of the changes in system response characteristics with changes in scanner geometry and design. Methods are developed to reduce the length of the fiber and make minor modifications to the tip of the fiber with the rest of the scanner system being intact. Thus a setup is developed that can cleave the fiber while the fiber is in the scanner and then the fiber tip is shaped to a flat geometry if required, using optical fiber polishing paper. The setup, as shown in Figure 14, consists of a fiber cleaving pen pushed down to cleave a fiber that is held onto a flat bed. The fiber is held down using tape which also allows to hold the fiber in some tension while it is being cleaved. Each of the three components on the setup in Figure 14 are mounted on XYZ stages which allows fiber to be cleaved by lengths as small as 0.6 mm.

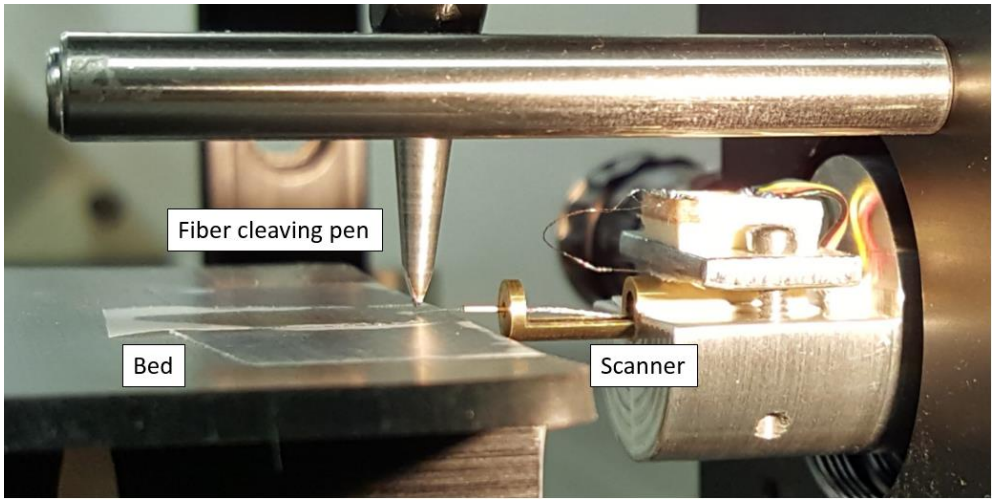

Figure 14: Fiber cleaving setup

Two other factors that affect the scanner is the shape of the cleaved tip and the integrity of the glass at the tip. Although these do not significantly affect the structural dynamics of the scanner, these affect the optics of the laser coming out of the scanner, which would then affect the data being collected to observe the structural behavior of the scanner. Thus several variations of this setup are tested, for example, by coarsely varying the amount of tension in the fiber, the angle between the fiber and the cleaving pen tip, the material of the flat bed, etc. until the most effective version that makes the minimal effect on the optical performance of the scanner is chosen. The commercial fiber cleaving instruments that can precisely hold and cleave the fibers could not be used for this study as they could not be used on the fiber while it was still in the scanner. Removing the fiber in order to be cleaved would involve disassembly and reassembly of the scanner, which could add a lot of variability to the system under test.

Figure 15 below shows examples of cleaved fiber tips. (a) is an example of a desired cleave that doesn't adversely affect the optical performance of the system. (b) is an example of a fiber tip that was cleaved along a flat plane, but ended up cracking/shattering the tip. The laser light throughput in this case may not be fine due to internal reflections. (c) is an example of a tip that has not cracked but the cut is not planar. In this case the fiber tip can be polished and get it to be more like (a). Polishing is done in two stages. First a coarser fiber polishing film with a surface made of 5 μm Silicon Carbide grits is used to polish the tip, followed by a finer polishing film with a surface made of 1 μm Aluminum Oxide grits. In case the cleaving process results in a tip similar to (c), this polishing step was able to bring it to a state closer to (a) and restore the optical performance of the system.

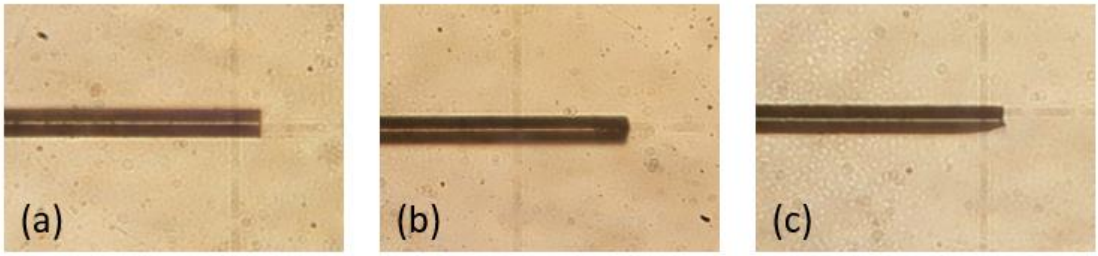

Figure 15: Examples of cleaved tip of fibers - (a) Ideal cleave, (b) Flat cleave but cracked fiber tip (c) Non-planar cleave

5. Coupled Model Validation

5.1. PSD Transfer Function

At this point, it is to be noted that the output of the simulations output is the actual position/ displacement of the fiber tip. Whereas in the case of the experimental system, the output is the position/displacement of the laser spot as it falls on the PSD. Although it is possible to estimate the fiber tip position from the experiments, this involves a manual step of measuring the deflection using the microscope and the XYZ stages. It is first noted that the actual fiber tip displacement estimated using manual measurement and software post-processing is proportional to the PSD output voltage across the near resonance frequency range, as shown in Figure 16. Thus the transfer function from the PSD output to the actual fiber tip displacement is a constant gain as long as the experimental setup and the system is not modified. As this study focuses on relative comparisons instead of absolute values, the rest of the study uses the relative change in these two terms interchangeably. The actual tip displacement from simulation results, scaled by the constant gain PSD transfer function is referred to as scaled tip displacement through the rest of the study and is given the units of Volt.

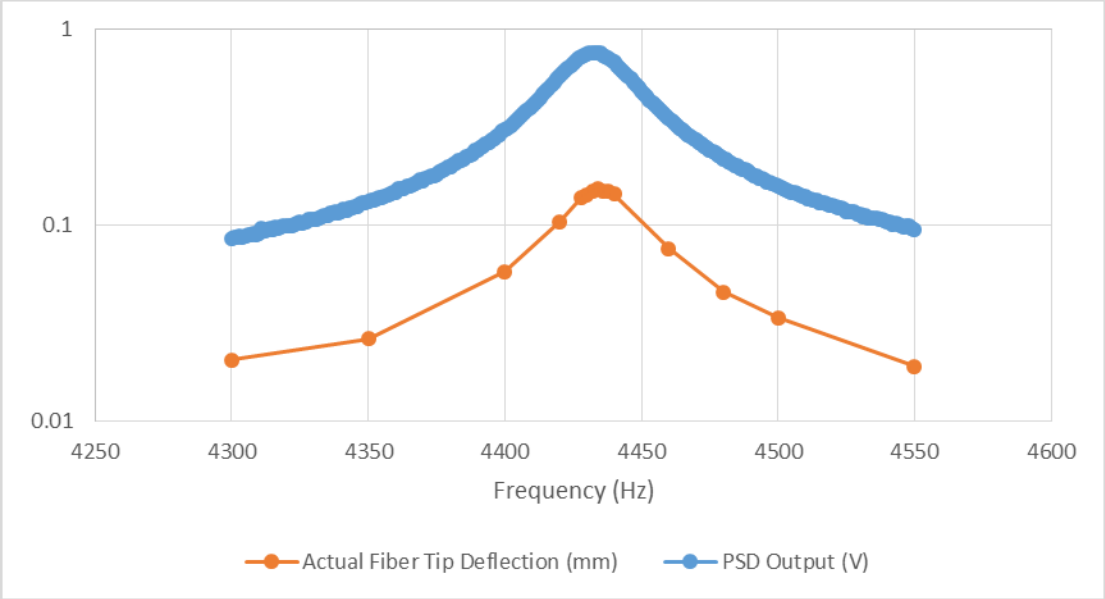

Figure 16: Comparison of the actual fiber tip deflection and Output voltage of the PSD

5.2. Linear Model Validation

5.2.1. Piezo-Tube Model Validation

The electromechanical coupled model developed as described in Section **Error! Reference source not found.** is validated in two steps. A scanner setup is tested on the Scan Drive Monitor with the fiber cleaved such that the fiber tip sits almost flushed with the piezo-tube. The frequency response and thus resonance frequency and Q factor of the system is obtained. The Q factor is used to tune the isotropic loss factor of the piezo-tube.

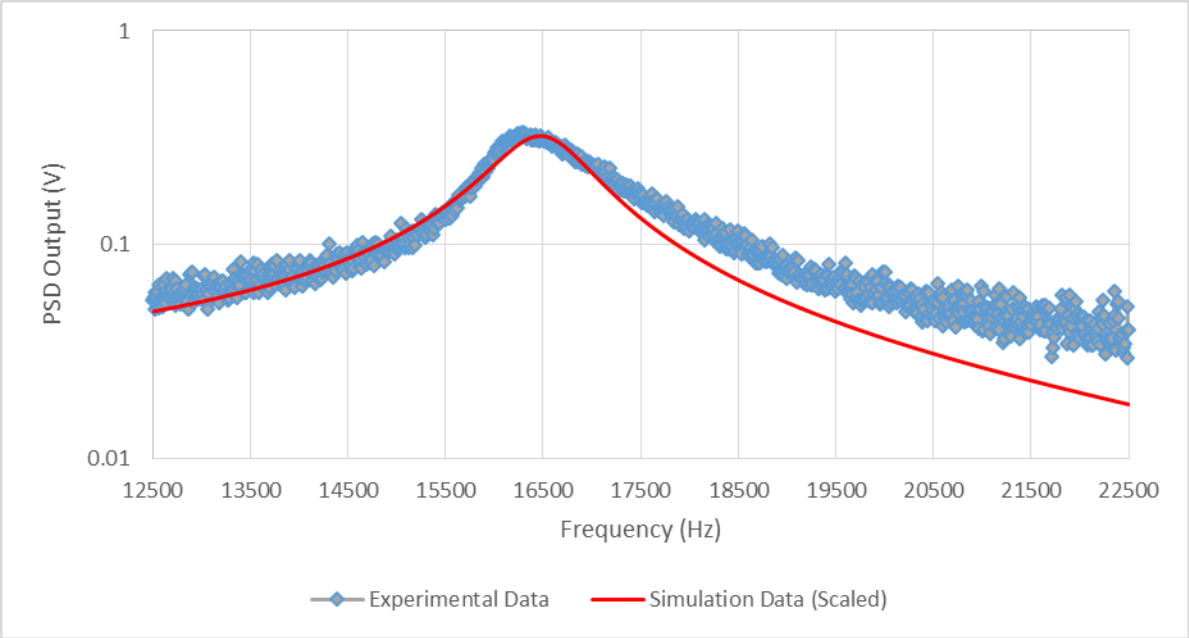

Figure 17: Validation of the system sans the fiber

5.2.2. Full System Model Validation

Next the complete scanner system model is validated using data from multiple sources. As production fiber scanner systems are usually driven at the first resonance mode of the fiber, the tuning and validation will also be mainly based on the frequency range around this resonance mode. First a set of data from experiments is used to tune the model. The results from tuning, as seen in Figure 18, show that the tuning has been successful and that both the modal and frequency domain solvers give almost identical results (overlapping curves in Figure 18) at least for a linear system response. As the modal solver is around 30 to 40 times faster than the frequency domain solver, the modal solver

will be used through the remainder of this study to estimate the frequency response of the coupled scanner model.

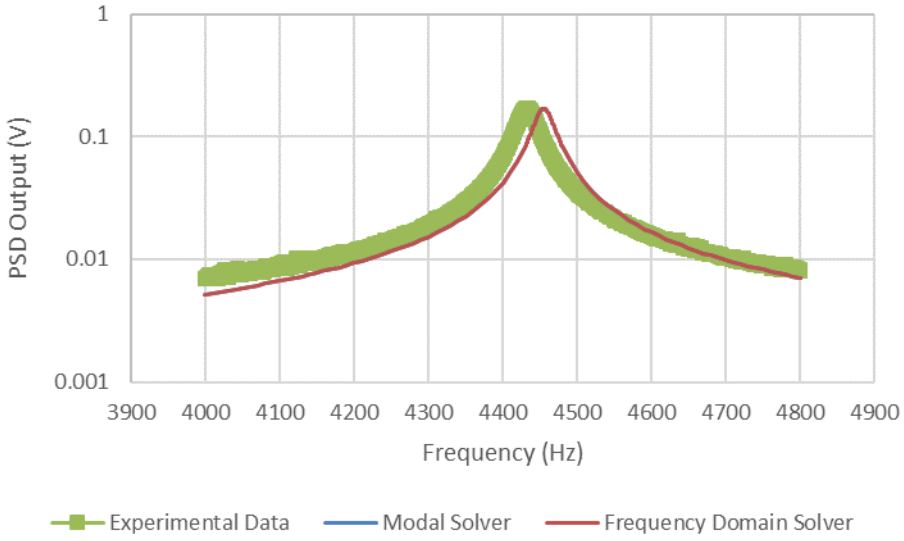

Figure 18: Frequency response of the tuned model as solved by Modal and frequency domain solvers compared against experimental data

The accuracy of the resonance frequency computed by the model is compared with resonance frequency computed from experiments and also with the resonance frequency computed using Euler Bernoulli beam theory.

The Euler Bernoulli (EB) beam model consists of only the fiber being modeled as a cantilever beam. The first natural frequency of a Euler Bernoulli beam is given by [22],

$$f_{res} = \frac{1.875^2}{2\pi}\sqrt{\frac{EI}{\rho A L^4}} \tag{5.1}$$

Here E is the elastic modulus, I is the second moment of cross-sectional area A and ρ is density. In order to model the fiber in this system as a Euler Beam, intuitively L would be the cantilevered length of the fiber, as shown in Figure 19. But as seen in Figure 20, the Euler Beam model provides more accurate results if L is chosen as the total length of the fiber in the model, that is the length of the fiber from the free end to the silicone ball.

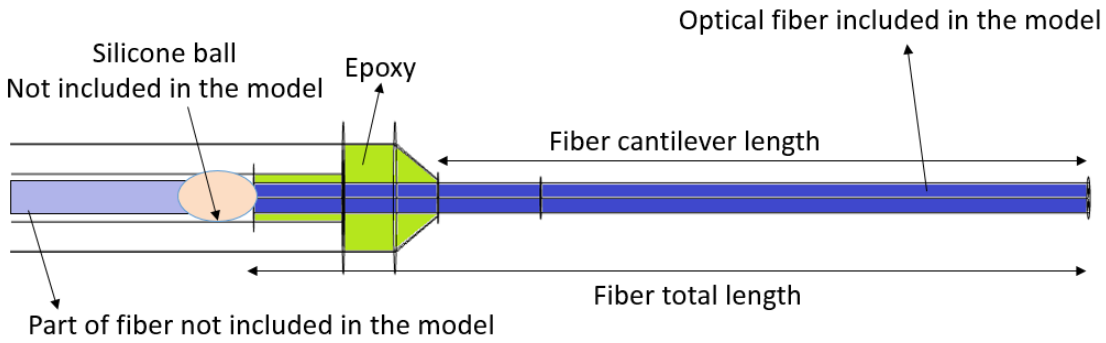

Figure 19: Cross-sectional view of the scanner

Thus the resonance frequency predicted by the coupled model developed in this study is seen to agree very well with experimental results, except for high frequency short fiber length scanners. This is because at high frequencies, the response of the scanner becomes highly non-linear, as explained later. Even for such scanners, Figure 20 shows that the coupled model is seen to follow the trend more closely than the Euler Bernoulli beam model. Here the excitation amplitude is kept very low in the experiment data set to keep the system linear. This study also notes that the modified Euler Bernoulli beam model with length being the fiber total length as in Figure 19 also gives good agreement with experimental data and could be a quick 'sanity check' for simulation results.

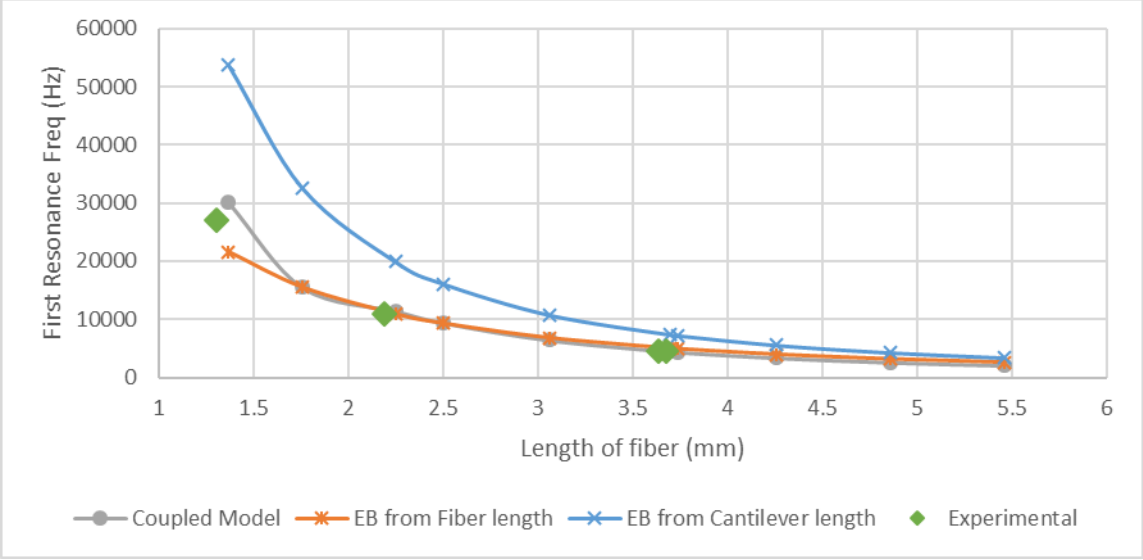

Figure 20: Comparison of Resonance Frequency from different models and from experiments

Tip deflection specifically is validated using data from [23], where axial change and rotation angle as illustrated in Figure 21 is compared to the same computed by the coupled model. The results show good agreement as seen in Figure 22.

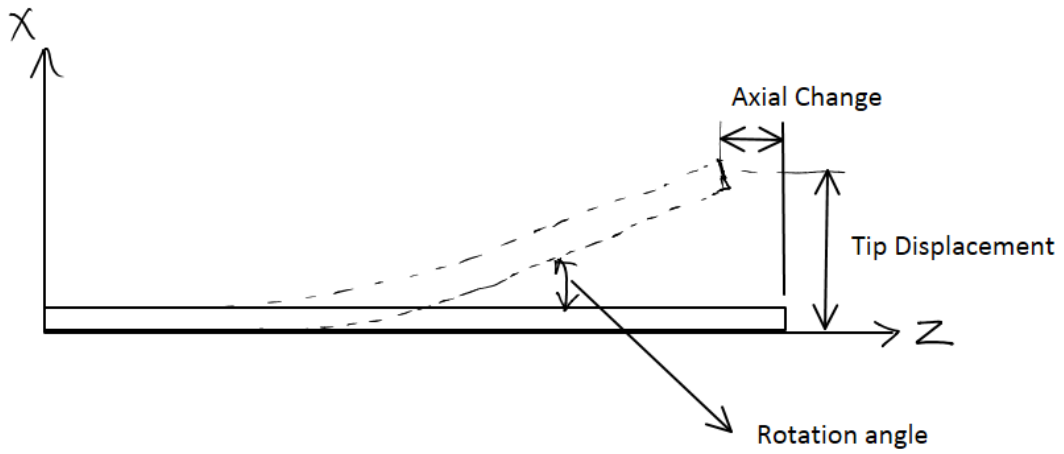

Figure 21: Illustration of system performance metrics being compared from [23]

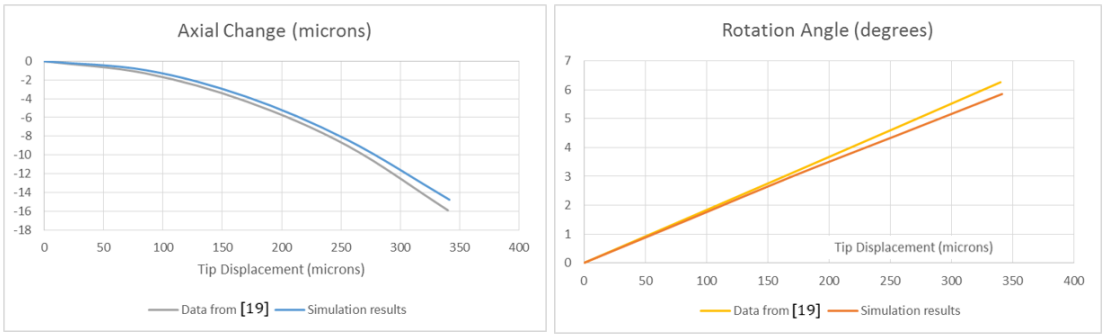

Figure 22: Comparison of data from [23]

5.3. Resonance Modes of the Scanner System

The coupled model was also used to identify the resonance modes of the system and verify if they match with the expected mode shapes. Due to the asymmetry in the geometry of the holder, the resonance frequencies of the scanner system would be different for excitation along x and y axes. This difference is minimal for the resonance mode of the fiber (~4 Hz) and much more significant for the resonance modes of the holder itself (~6000 Hz). Figure 23 (a) and (b) show the resonance modes of the scanner system due to resonance of the fiber. The frequency range around these modes are the main operating region for the scanner system and provide maximum amplitude fiber tip displacement.

For the scanner system used for the experiments it was seen that the uncoupled virtual electrodes of the system (as explained in [7] or Section 6.3) is along the y-direction. It was also desirable to have the fiber vibrate more along the y-direction, so that the fiber deflection can be measured more accurately using the Drive Monitor setup explained in Section 4.1. In this case the scanner system would be vibrating in the resonance mode shown Figure 23 (b). These two mode shapes match the mode shapes expected out of such systems from past experience.

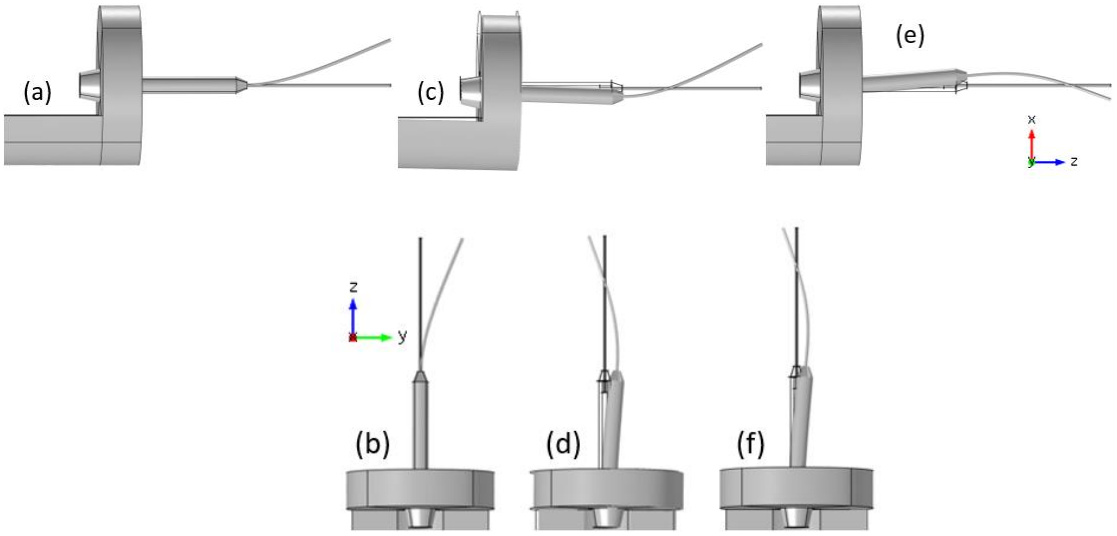

Figure 23: Resonance modes of the fiber scanner system

The holder and piezo-tube has not been extensively modeled before and thus are not validated. The resonance modes of the holder are shown in Figure 23 (c) and (d). Due to the asymmetry of the holder these are around 5 kHz and 11 kHz respectively. The resonance modes of the piezo-tube are shown in (e) and (f) and are around 16 kHz.

6. Experimental Data Analysis

6.1. Non-Linear System Response

The fiber scanner system can show a non-linear frequency response under certain design and actuation conditions. For example, when actuation amplitude is increased a combination of material non-linearities in the piezoelectric material and the geometric non-linearities attributed to large deformations, could cause the system response to shift towards lower frequencies [24]. One of the forms in which non-linearity is exhibited is through the 'jump' phenomenon [25] where the frequency response magnitude makes a discontinuous jump from at critical frequency during an increasing frequency (forward) sweep and a different discontinuous jump during a decreasing frequency (reverse) sweep. This can be seen in Figure 24 below. This behavior is similar to that of a damped Duffing oscillator and the jump happens due to the presence of an unstable region for the linear system between the two end of the jump [25] which the system avoids. This leads to various consequences to the system performance, which will be explored in this section. This section also studies the effect of three factors - actuation amplitude, fiber to piezo-tube CA joint shape and fiber length - on this non-linearity in the frequency response of the system.

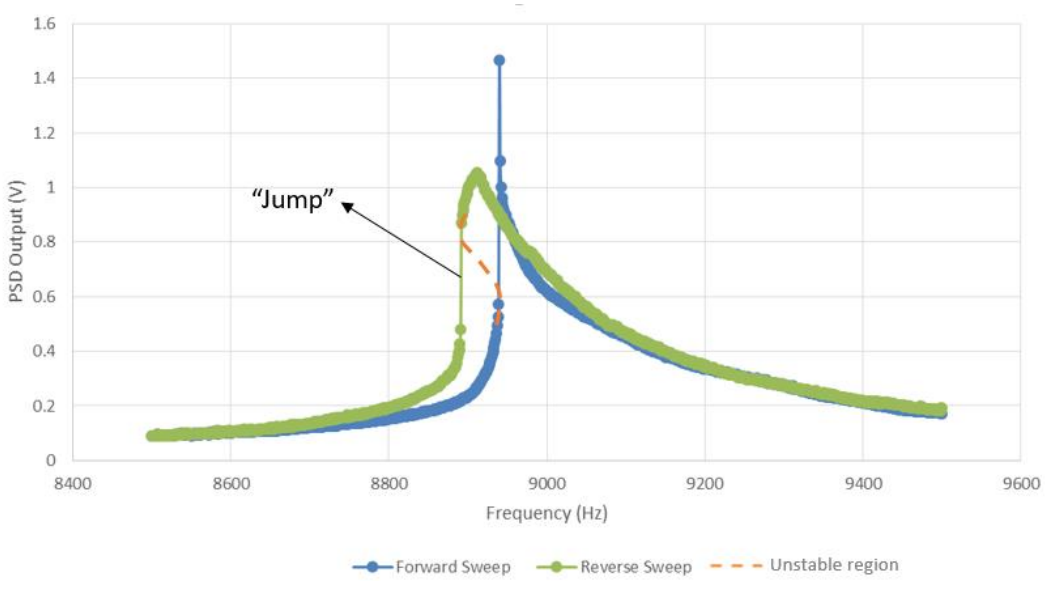

Figure 24: Experimental data from the scanner system showing jump phenomenon

Although there are several factors that can push the scanner design to be more non-linear, due to practical constraints, this study chooses to look at three main factors. These factors are chosen on the basis that they are very much design choices made at relatively the final part of the assembly of a probe instead of being an implicit material property. Thus these could be varied independently of the rest of the system which helps in developing better correlation between the factor and the non-linearity. As making the required variations in the system involved cleaving the fibers and dissolution and recurring of the CA joint, two separate assemblies of the scanner system are used. The first system is assembled tested through varying fiber lengths and then disassembled. Then a new optical fiber from the same spool of fibers is processed and assembled into the system replacing the older one. Then the CA joint is remade with a second design. The former and latter fibers will henceforth be called fiber 1 and fiber 2 respectively.

6.1.1. Actuation amplitude

The system is actuated through the drive voltages that are input to the piezo-tube. It is seen that the non-linearity of the system increases as the drive voltage is increased. This may be because of geometric non-linearities becoming more significant at larger amplitudes and deflections. It is also known that the damping in viscoelastic materials vary with strain amplitudes at high frequencies [26].

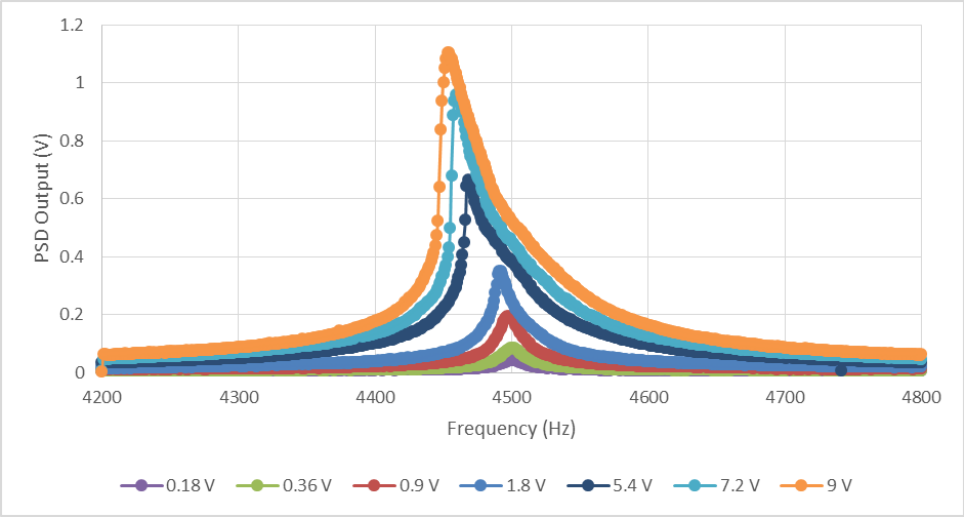

Figure 25: System with fiber 1 transitioning from linear to non-linear as drive voltage is increased

But the biggest contributor could be the inherent non-linearity in the piezoelectric material. This is because minor non-linear behavior is visible even in the scanner system described in Section 5.2.1, with the fiber flushed to the end of the piezo-tube. Also previous studies like [27] have reported non-linear behavior for a micro-cantilever system actuated by a piezoelectric layer and does not contain any viscoelastic domains.

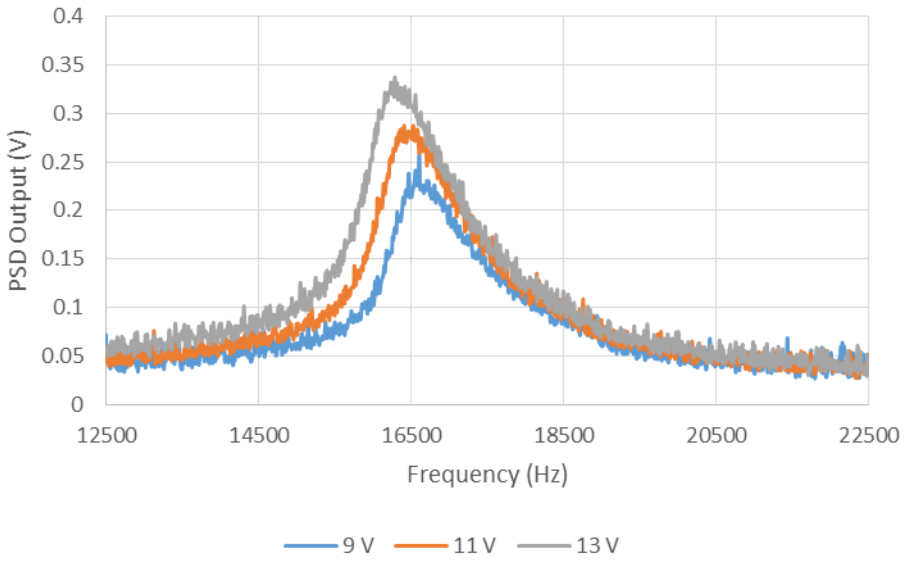

Figure 26: System with fiber flushed to the piezo-tube displaying increasing non-linear behavior as drive voltage is increased around resonance mode of the piezo-tube

6.1.2. CA Joint

Two different designs (Figure 27) of the CA joint are compared and their effect on system performance is analyzed. The design of the CA joint is one of the factors that is the most difficult to control effectively during scanner system assembly. To make the CA joint, the piezo-tube and fiber are positioned as per the required design and then cyanoacrylate (CA) glue is applied on the joint. Some of this glue gets pulled into the piezo-tube as shown in Figure 19 in Section 5.2.2, due to surface tension effects. Thus the amount of glue deposited on the joint, the surface tension, contact angle, density of the glue and how fast the glue cures all affect the amount of glue on the inside and outside of the piezo-tube. Some control can be achieved over this process by choosing the glue with an appropriate cure time, carefully controlling the amount of glue applied and then ensuring that there are no drastic changes in the temperature and humidity of the air local to the glue being

cured. From past experiences building scanners, it is believed that the design in (a) in Figure 27 is a result of the CA glue getting pulled into the piezo-tube and less of it visible outside. The design in (b) is a result of the CA glue curing faster than the ability of capillary action to pull the glue into the piezo-tube.

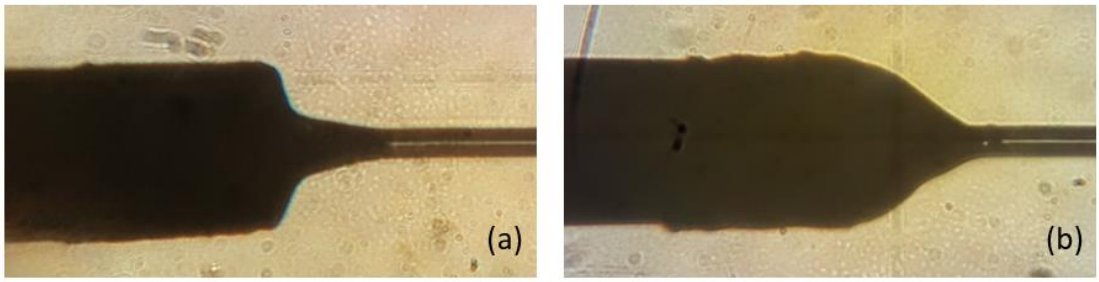

Figure 27: Microscope images of the silhouettes of the CA joint which holds the fiber to the piezo-tube

The experimentally determined frequency response of scanner systems with the two CA joint designs is shown in Figure 28. It is to be noted that in order to change the CA joint design, the fiber had to be removed and reassembled. Due to human error the lengths of the fiber that is cantilevered out of the piezo-tube does not exactly match between the two designs. With design (b) ending up with a slightly shorter fiber cantilever length, this has caused the resonance frequency to shift slightly right. Aside from that design (b) is shown to exhibit a non-linear behavior whereas design (a) shows a linear behavior. This pattern is continued for all ranges of input drive voltages that are tested. During testing it was observed that design (a) (with more epoxy inside the piezo-tube) had a longer 'break-in' period. But after that, both the scanner designs had similar fiber tip deflection amplitudes. Thus it might be desirable to have a CA joint design similar to (a) in order to avoid a harder to control non-linear system.

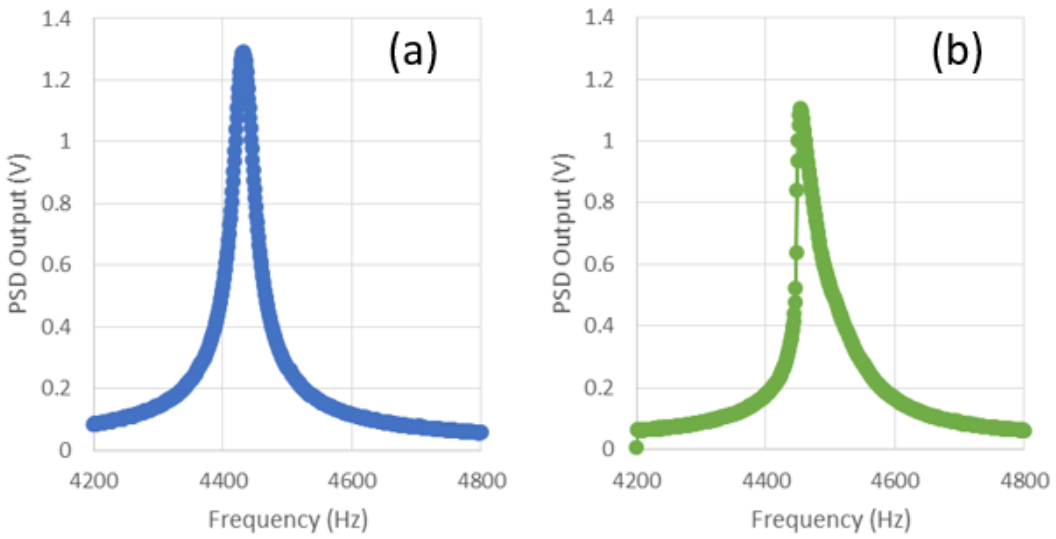

Figure 28: Frequency response of the two CA joint designs (a) and (b) near the first resonance mode when actuated to have similar fiber tip deflection

6.1.3. Fiber length

Two strands of optical fibers, from the same spool of fiber was used in this study. The first fiber strand is cleaved, polished and tested twice and then removed from the scanner assembly and replaced with the second fiber strand. The second fiber then went through a similar process. These two strands will be referred to as fiber 1 and fiber 2 respectively for the rest of the study.

It is to be noted that due to some unfortunate events during the duration of this study, the piezo-tube being used was damaged. Thus a second piezo-tube from the same batch was used for the rest of the study. The second piezo-tube is geometrically the same. But as the piezo-tubes are known to have a lot of variability, there might have been some difference in performance between the two. All data being compared in this section has fiber 1 using the original piezo-tube and fiber 2 using the second piezo-tube.

The CA joint is also different between fibers 1 and 2, with the former made as per design (b) in Figure 27 above and fiber 2 using design (a). This was done so that one of the data sets included a linear to non-linear transition as the fiber length is reduced.

Due to these variations between the systems used for fiber 1 and 2, this study refrains from comparing the results from fiber 1 and 2. Instead this study will look at the trend in

each of those data sets separately. Figure 29 and Figure 30 show the variation in frequency response as the length is varied. A change in fiber length also changes the resonance frequency. In order to help with data visualization, the frequency response is plot with respect to a normalized frequency which is the ratio of input drive frequency to the resonance frequency of the scanner system with that particular fiber length. It is also to be noted that the frequency response is that of the output voltage from the PSD. As mentioned in Section 5.1, the PSD output voltage is related to the actual fiber tip displacement through a PSD transfer function. But this could have varied due to changes in the tip geometry during cleaving and polishing, refocusing of the laser on the PSD by lens adjustments, etc. Thus the plots may not represent the relative change in fiber tip displacement and are to be used to look at the relative increase in non-linearity as the fiber length is reduced. This can be seen from the 'jumps' being higher for shorter fiber lengths. In summary, the plots show that despite the difference between the scanner systems used for fiber 1 and fiber 2, the trend is the same, that is non-linearity is seen to become more significant as the fiber length is reduced.

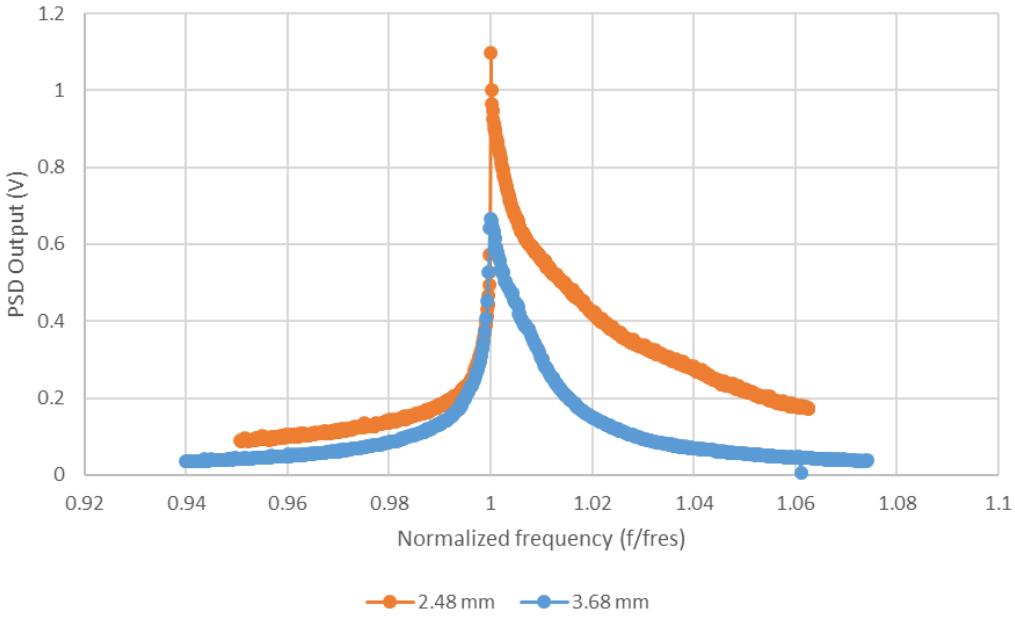

Figure 29: Response of the system with varying fiber 1 lengths at the same input drive voltage of 5.4 V

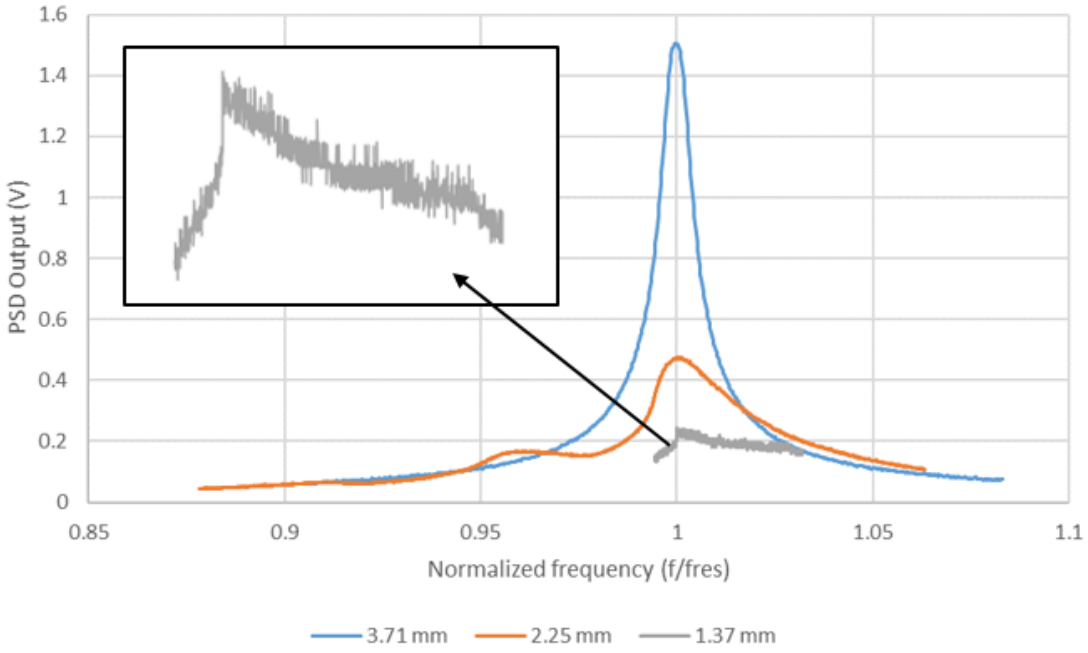

Figure 30: Response of the system with varying fiber 2 lengths at the same input drive voltage of 13 V

As seen above the scanner system can transition from linear to non-linear due to various factors. Larger actuation voltages can lead to larger deflections which could increase the imaging or display area of the scanner system. In this regard, driving the system in a non-linear operating region could be desirable. But this would then add more challenges to being able to accurately control the system due to additional variability added due to non-linear effects. More research needs to be done before analyzing the controllability, advantages and disadvantages of the two operating regions.

6.2. Tip Displacement Amplitudes

One of the crucial performance metric for the scanner system is the amplitude of the tip displacement. For a production scanner, this is one of the factors that defines the field of view (for an imaging probe) or display area (for a display probe). This section explores how the tip displacement varies with respect to the input drive voltage and also the length of the fiber. The correlation from the coupled model is also explored. As explained in Section 4.1, manual measurements of the actual fiber tip deflection are made for each input drive voltage amplitude. Here again two data sets are compared. The first data set

is the coupled model and experimental data of a linear system which consists of a 3.7 mm fiber cantilever scanner with a CA joint design as in (a) of Figure 27 and the second piezo-tube as mentioned in Section 6.1.3 henceforth referred to as scanner 1. The second data set is the coupled model and experimental data of a non-linear system which consists of a 2.25 mm fiber cantilever scanner with the same CA joint and piezo-tube, which will be referred to as scanner 2. Fiber tip deflection predictions of the coupled model simulation results of scanner 1 is close to the experimental data with an error around 10% even for scanner peak to peak deflections of about 700 microns (Figure 31).

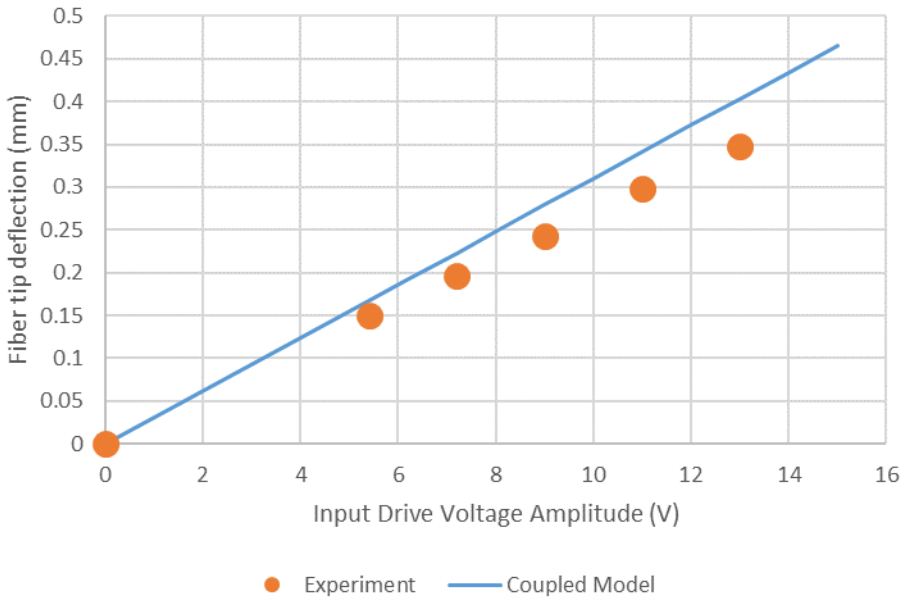

Figure 31: Variation of fiber tip displacement amplitude with respect to input drive voltage amplitude in simulation and experimental data for scanner 1

Unlike scanner 1, scanner 2 has a non-linear response, as seen in Figure 30. Thus the error in this case is much higher averaging around 40%. Comparison is shown in Figure 32.

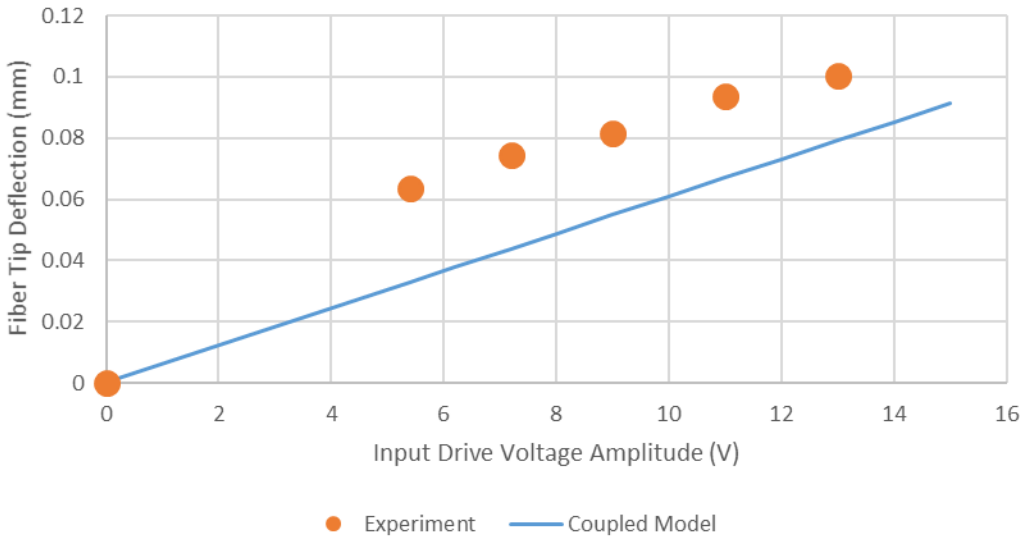

Figure 32: Variation of fiber tip displacement with respect to input drive voltage amplitude in simulation and experimental data for scanner 2

6.3. Scanner Characterization

This study has developed software and hardware, introduced in Section 4.1 that can be used to characterize and test a scanner assembly before it is shipped out of house. Some of the characteristic features have already been shown in the previous sections including the fiber tip displacement and the first mode resonance frequency. It has been previously shown that each sample of the piezo-tube has its own virtual electrodes. These are defined as two pairs of electrode surfaces on the piezo-tube such that if the input actuation is applied in these two directions then the fiber vibration will be uncoupled in the two orthogonal directions [7]. These two directions are a linear combination of the electric field that would be setup by actuating the actual electrodes on the piezo-tube. The linear combination can be written out as,

$$V_{VE1}(t) = f(t)\sin(\omega t)[sin\theta_1\widehat{x_1} + cos\theta_1\widehat{x_2}] \quad (6.1)$$

$$V_{VE2}(t) = f(t)\cos(\omega t)[cos\theta_1\widehat{x_1} + sin\theta_2\widehat{x_2}]$$

$$0 < \theta_1 < \pi/2 \text{ and } \pi/2 < \theta_2 < \pi$$

If it is desired to achieve whirl free excitation as it usually is, these two angles are controlled such that if the piezo-tube is actuated along the direction of one of the pairs of virtual electrodes, then the fiber vibrates in a straight line. The scan being in a straight line is recognized in software by the circularity of the scan approaching zero. Software

was developed in LabVIEW and MATLAB to estimate the θ_1, θ_2 corresponding to the virtual electrode directions. An example is shown in Figure 33.

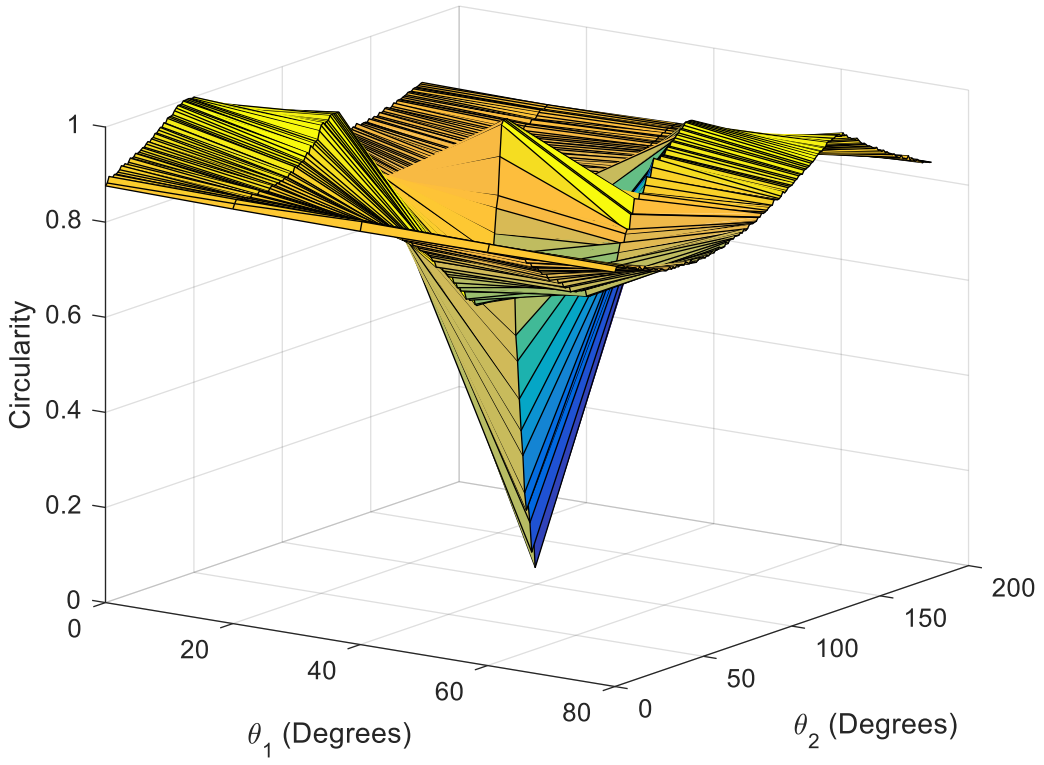

Figure 33: An example of variation in circularity with changes in scan parameters

7. Reduced Order Models

7.1. Transfer function based models

Accurate estimation of transfer function based models of the scanner system are essential for developing efficient control systems for the scanner. When it comes to performance of the scanner systems, the output that needs to be controlled is the deflection of the fiber tip. But presently there are no methods to measure the fiber tip deflection for a production scanner in order to obtain the transfer function from input to output. In previous works the frequency response of the self-sensing voltage from the piezo-tube was measured experimentally, which was then used to estimate a transfer function for the scanner system [28] and then used to control the actual output of the scanner system using concepts from modern control theory.

The availability of a validated coupled model can enable more accurate estimation of any system variable, including the fiber tip deflection amplitude and phase. As described in Section 3.3 above, these results from the coupled model is used to estimate a reduced order transfer function for the scanner system. As the order of the transfer function can be arbitrary, a multi-parameter sweep was performed to locate the best estimate. The results, shown in Figure 34, show that the best fit to output from the coupled model is would be a transfer function with 4 poles and 2 zeros.

Next an initial guess for a transfer function of this order is provided to the algorithm described in Section 3.3. The transfer function estimate with less than 5% error, thus obtained is,

$$\frac{U(s)}{V_{in}} = \frac{-7.64 \times 10^5 s^2 - 1.3 \times 10^{10} s + 7.77 \times 10^{15}}{s^4 + 3268 s^3 + 1.14 \times 10^{10} + 4.35 \times 10^{12} s + 8.3 \times 10^{18}} \qquad (7.1)$$

The frequency response of this transfer function is compared to that of the coupled model in Figure 35. The most significant resonance modes of the system are the first resonance modes of the fiber ($4456\ Hz \approx 28000\ rad/s$) and piezo-tube ($16346\ Hz \approx 10^5\ rad/s$). Results show that the estimated tranasfer function exhibits frequency domain behavior close to the coupled model in this frequency range. The response of the coupled model in the frequency range of the first resonance mode has already been validated in Section

5.2.2 With more experimental data in the higher frequency region, the coupled model can be tuned further for high frequencies which can in turn be used for estimating a transfer function that is more accurate at higher frequencies. In the figure it is to be noted that the phase plots are just offset by 360°, which amounts to being the same.

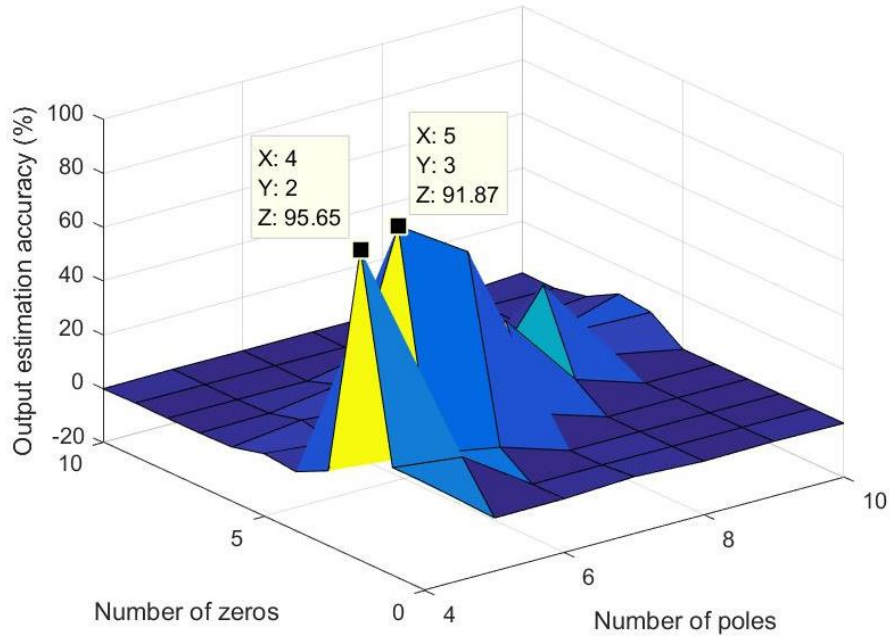

Figure 34: Search for order of maximum accuracy transfer function estimate

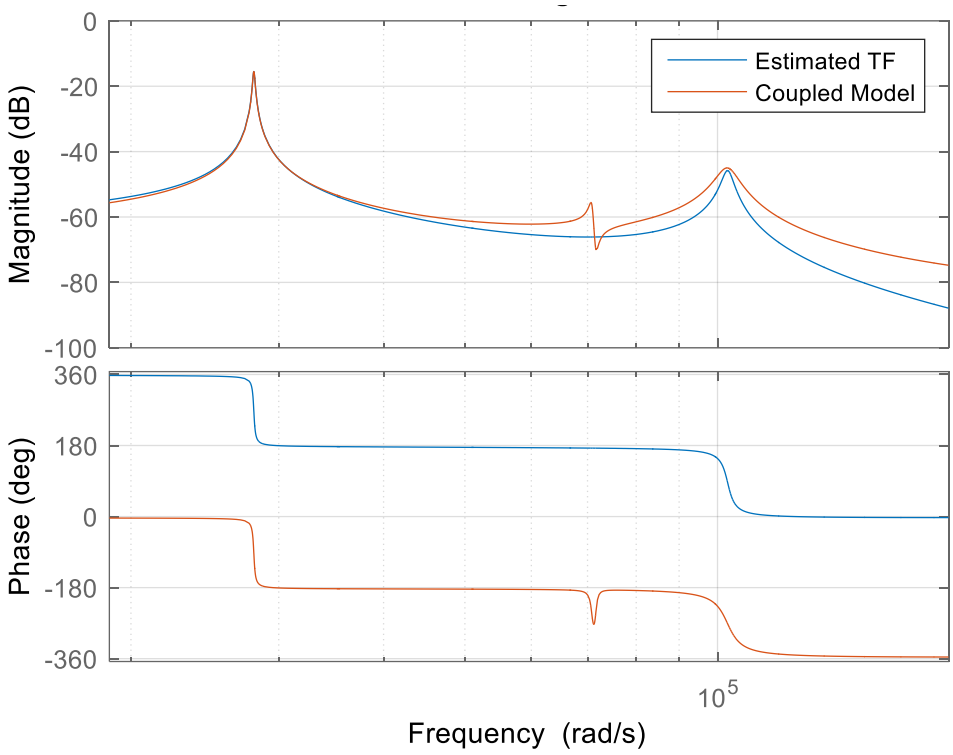

Figure 35: Frequency response of the estimated transfer function compared to the coupled model's frequency response

7.2. Reduced Order Non-Linear Model

From the experimental data presented in Section 6.1, it can be seen that the scanner system can exhibit non-linear frequency response for certain design and actuation conditions. It is also highly advantageous to predict if a particular design is going to be linear or non-linear, early in the design stages. This non-linearity is believed to be from four sources:

- Studies have reported that the dielectric, elastic and piezoelectric coefficients of ferroelectric ceramics vary based on the stress and electric field in the material [29]. These also exhibit creep behavior due to the slow realignment of the polarized domains in the applied external electric field over time [30]. As mentioned in Section 3.1.2. There is also a hysteresis between the electric field and polarization in such materials. The material model used in the coupled model is based on the linear constitutive equations for piezoelectric materials.

- Viscoelastic materials, including the cyanoacrylate used in the scanner system show a variation in the complex modulus with respect to time/frequency due to stress relaxation [26]. For high frequency applications such as this scanner system, this behavior is also believed to be dependent on the strain amplitude in the viscoelastic material, which would then be related to the actuation amplitudes. As mentioned in Section 3.1 the cyanoacrylate is modeled as a linear elastic material in this study.
- Fiber displacements that are relatively much larger than the fiber dimensions also lead to effects of geometric non-linearity in the equations of motion. Although COMSOL software used in this study is able to model geometric non-linearity, the frequency domain and modal solvers outlined in Section 3.2.3 require the system to be linearized about an operating point before being solved. Thus the coupled model developed in this study is unable to capture the non-linearity due to the large deflections in frequency domain.
- It is also possible that the vibrating fiber experiences viscous effects due to air damping. But previous in-house tests showed some evidence to indicate that this effect is not very significant.

Thus to simulate non-linearity in the fiber scanner system using the developed coupled model is to solve the model in time domain with a sinusoidal input of a certain frequency until the system reaches steady oscillations. Then record the amplitude of these steady state oscillations and then restart the time domain simulation with the next frequency. Such a parametric sweep of input frequency over time domain simulations for such a high fidelity finite element model was seen to be very computationally demanding and would take multiple days to complete. As the reduced order transfer function estimated in Section 7.1 has shown a good level of accuracy at the same time being much faster than the coupled model, this section explores using this reduced model to develop non-linear reduced order models of the scanner system.

The estimated transfer function given in (7.1) consists of 4 poles and 2 zeros which are highlighted in Table 1. It can be seen that the first pole pair corresponds to the first resonance mode of the fiber and the main operating point of the scanner system. As

transfer functions are linear, these two modes can be separated out of the system into a separate transfer function given by,

$$H_f(s) = \frac{1}{s^2 + 182.1s + 7.851 \times 10^8} \tag{7.2}$$

This leaves us with a second order damped harmonic oscillator subsystem of the form,

$$\ddot{x} + 182.1\dot{x} + 7.851 \times 10^8 x = F \tag{7.3}$$

Here x is the displacement of the oscillator and F is the force input into the system. Even though non-linearities exist in different parts of the scanner system, the idea here is to modify this subsystem to represent a lumped non-linear model that can model the overall non-linearity seen in the experimental data.

Table 1: Poles and zeros of the estimated transfer function

Type and number	Location in complex plane	Frequency (Hz)
Pole 1	-91.04+28019.02i	4459.36
Pole 2	-91.04-28019.02i	4459.36
Pole 3	-1542.72+102822.24i	16364.67
Pole 4	-1542.72-102822.24i	16364.67
Zero 1	-109685.39	0
Zero 2	92670.79	0

This is done by modifying (7.3) by adding a non-linear term which results in,

$$\ddot{x} + 182.1\dot{x} + 7.851 \times 10^8 x - \psi g(x) = F \tag{7.4}$$

Here ψ is the measure of non-linearity in the system and is estimated from the set of tuning data and is a positive real number. A cubic form of g(x) is seen to give good correlation with experimental data as shown in Figure 36. As the point is to compare the general shape, the x and y axes are normalized frequency and fiber tip displacement amplitudes, respectively. A cubic form of g(x) in (7.4) is the state equation for a damped Duffing oscillator.

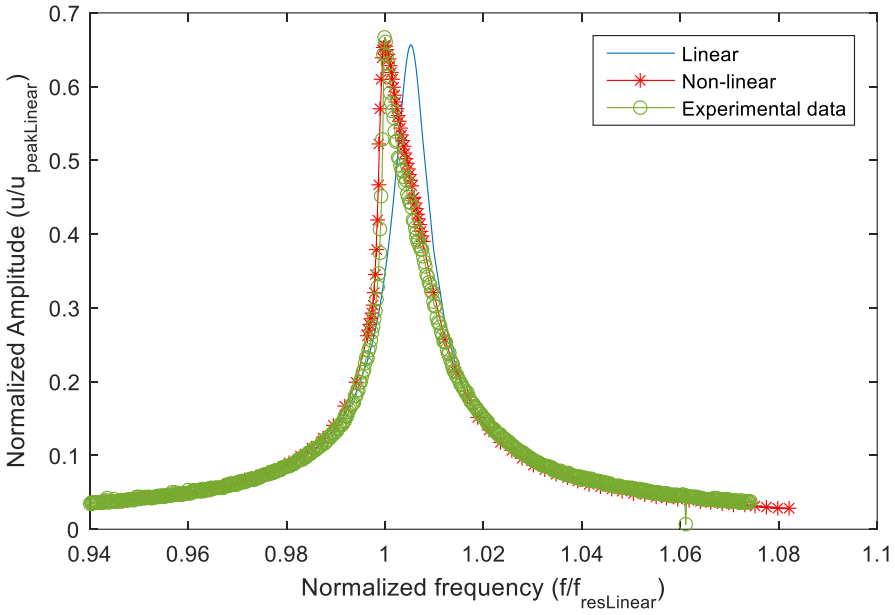

Figure 36: Tuned Non-linear and tuned linear reduced order models compared with experimental data

The coupled model being linear, does not capture the variation in resonance frequency as the input drive voltage amplitude is increased. The reduced order non-linear model is able to, as shown in Figure 37. This figure uses the same experimental data presented as frequency response plots in Figure 25 earlier.

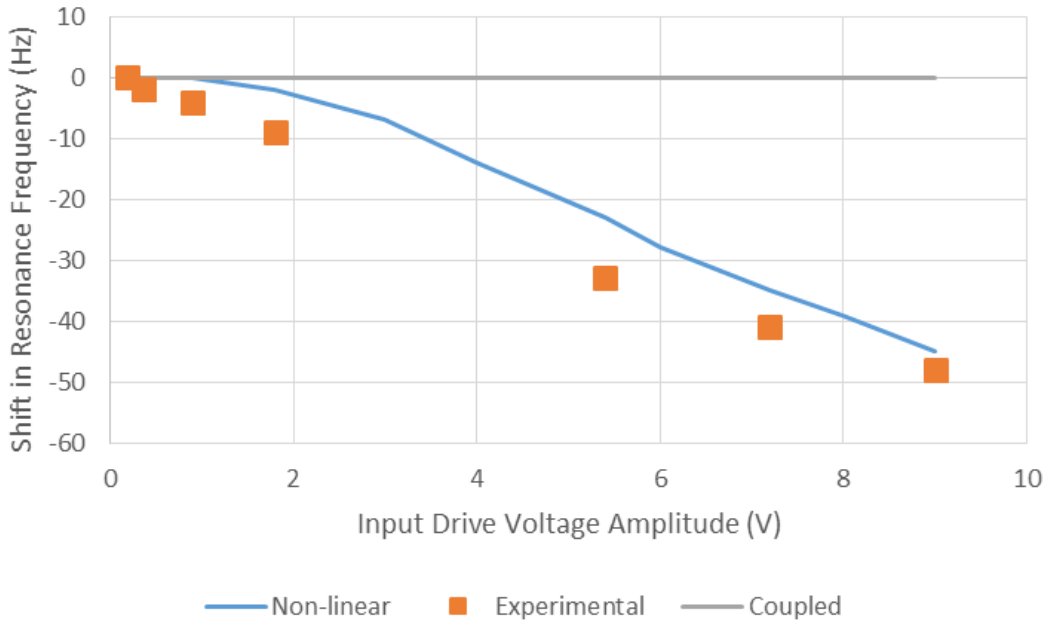

Figure 37: Shift in resonance frequency as the input drive voltage amplitude is increased

8. Model Based Design of Scanner Systems

This study has developed a high fidelity electromechanical coupled model for a fiber scanner system and validated it in the primary operating region around the first resonance mode of the fiber. This section outlines some of the studies done with the coupled model to explore the relative change in scanner performance with respect to changes to certain design parameters.

8.1. Piezo-tube Non-Circularity

There are significant variations in the manufacture of the piezo-tube and the dynamics of the tube vary sometimes within the same batch. Even though the quality control has improved drastically, this still contributes to a major share of the deviation in the system produced from the system designed. The gain from voltage to deflection and the non-circularity in the geometry of the piezo-tube varies from sample to sample. A sensitivity analysis was performed to understand the effect of this non-circularity on the first resonance mode of the fiber. The amount of non-circularity in the system is correlated using the inverse of an aspect ratio factor for an ellipse defined as,

$$א = \frac{length\ of\ minor\ axis}{length\ of\ major\ axis} \tag{8.1}$$

Thus a value of 1 would correspond to a perfect circle and a value of zero would correspond to a straight line. Unless the piezo-tube is perfectly circular, which under real life conditions is never the case, there would be two resonance frequencies for the scanner system due to this asymmetry. All through this study it was assumed that the piezo-tube is perfectly circular. Figure 38 shows the absolute value of the difference in frequency between the two resonance peaks. Such sensitivity analysis data can be used to perform quality control for commercial level manufacturing. Based on the level of non-circularity in the piezo-tube samples that are used, the control systems for the scanner can be built to handle such variations in resonance peaks.

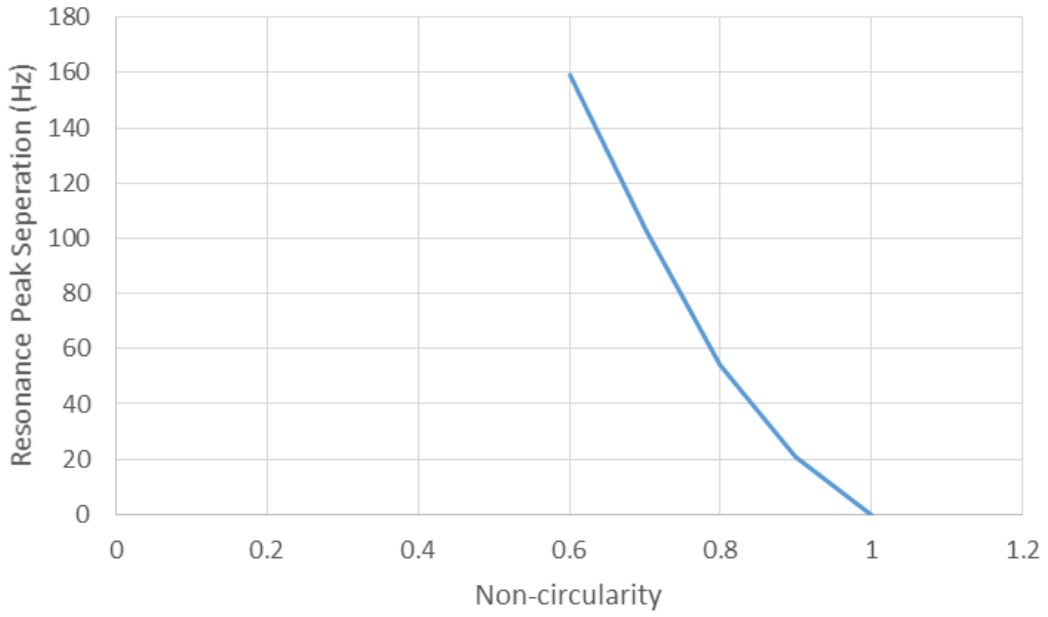

Figure 38: Separation of the first resonance peak as the non-circularity defined in (8.1) is increased

8.2. Etched Fiber Designs

Previous studies have shown that etching parts of the fiber cantilever to reduced diameter regions, can increase flexibility and thus the fiber tip deflection amplitudes [31]. As these are higher amplitude fiber displacements, it is likely that the system would behave non-linearly. Even then the coupled model developed here can be used to estimate the first resonance mode frequency of an etched fiber, which may not be very intuitive. For example, if the design challenge is to come up with a design for an etched fiber with the same fiber length as a non-etched 3.7 mm fiber with similar resonance frequency and double the fiber tip displacement at resonance, the coupled model can be used to get initial designs for a scanner which would perform close to the target specifications. In case the fiber tip deflection prediction of the coupled model is found to be inaccurate when the etched fiber scanner is built, that can be rectified by increasing the input drive voltage amplitudes.

Figure 39: Etched fiber design

The etched fiber design that will be simulated in this study is shown in Figure 39. A parameter called etch fraction ξ is defined such that,

$$\xi = \frac{l_{f2}}{l_{f1} + l_{f2}} \tag{8.2}$$

Thus the percentage of this fraction would be the etch length percentage. The diameter of the l_{f1} section of the fiber would be the original 80 μm and the diameter of the etched l_{f2} section of the fiber would be 40 μm. Variation of resonance frequency and fiber tip displacement with respect to etch fraction or percentage is shown in Figure 40. The resonance frequency first increases and then decreases as the first mode of resonance of the etched fiber transitions from the l_{f1} section of the fiber to the l_{f2} section of this fiber. This is accompanied by a relatively large rise in fiber tip deflection as the system moves into the resonance mode of the more flexible part of the fiber.

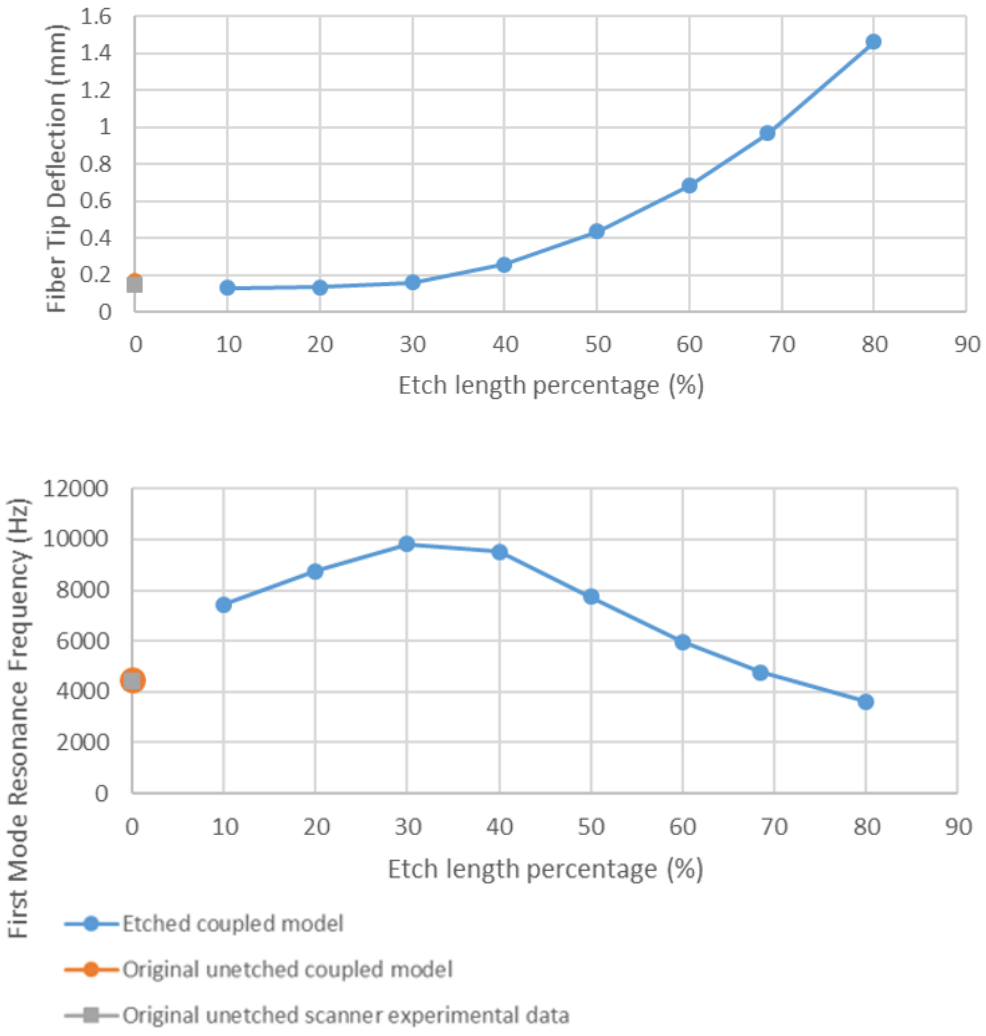

Figure 40: Variation in resonance frequency and fiber tip deflection as etch length percentage is increased

9. Conclusions

This study has developed a unique model that uses the electromechanical model of piezoelectric materials and also includes the different components of a fiber scanner system along with the coupling between these components. The electromechanical model allows simulations that includes the model being actuated electrically while looking at the mechanical deformations. Such models haven't been developed before for these fiber scanner systems. The coupled model also allows us to simulate changes at a component level, in geometry or material properties and analyze changes in the overall system characteristics due to these variations. Such a model based design approach to compare the effect of design choices on the system characteristics also hasn't been developed before. These models can be very valuable for projects planned for the near future which involves studying the effect of unconventional fiber geometry designs.

The study also included development of a testing station and data acquired from this station was used to perform validation of some aspects of the coupled model developed. Specifically, the resonance frequency of the system and the fiber tip deflection was compared with experimental data. For a linear scanner system, it was seen that the model is able to predict resonance frequency very accurately with no tuning when compared to previous models. For a non-linear scanner system, the linear system is unable to capture the shift in resonance frequency due to changes in actuation amplitude. Thus reduced order models are derived from the coupled initially developed. Then non-linearities are added to certain modes of the system resulting in non-linear reduced order models which are then able to predict such resonance frequency shifts. Thus with the un-tuned coupled model and the non-linear system with one set of tuning data, a system has been developed that can predict the resonance frequency of a scanner to good accuracy which can then be used to design scanners that would operate at customer desired frequencies. Fiber tip deflection is also estimated using the coupled model and compared with experimental data. It is seen that for a linear system with one set of tuning data, the coupled model is able to estimate fiber tip deflection to a good extent, but for a non-linear system with no retuning, the error can go up to 50%. This despite being a setback to the effectiveness of the model can be worked around in the actual scanner design-build process. Once the scanner is built and is seen to be under or over performing, the excitation voltage

amplitude can be increases or decreased to get the scanner to have the desired fiber tip displacement.

Lastly this study also takes a more in-depth look at the linear to non-linear transitioning of the system and finds that a test system with almost no fiber cantilevered out of the piezo-tube is still non-linear. Also it is seen that decreasing the length of the fiber, that is reducing the contribution due to the mass and stiffness of the fiber on the dynamics of the overall scanner system, makes the system more non-linear. These observations are used to come up with the hypothesis that the non-linearity in the scanner system is due to the piezo-tube and/or the adhesive joints at least for the fiber geometries that were used in this study. More research needs to be done to isolate the effects of the viscoelastic adhesive domains in order to estimate if these contribute significantly to the non-linearity of the system. This can help design scanners which aren't very non-linear which can then optimize the performance as the reduced order transfer functions used in control of the scanners would better represent the linear system. The study also demonstrates effects of changes in geometry on system characteristics. The capability of the model to predict effects due to geometry changes can be used to come up with better designs for the scanning fiber.

10. References

[1] C. J. E. T. D. S. F. H. a. E. J. S. Cameron M. Lee, "Scanning fiber endoscopy with highly flexible, 1 mm catheterscopes for wide-field, full-color imaging," *Journal of Biophotonics,* vol. 3, no. 5-6, pp. 385-407, 2010.

[2] E. Seibel, Interviewee, *Scanning Fiber Endoscopy -- Multimodes of Guided Intervention.* [Interview]. 27 May 2014.

[3] L. G. Paolo Maria Mariano, Fundamentals of the Mechanics of Solids, Birkhäuser Basel, 2015.

[4] "Brass Mechanical Properties," E-Z LOK, [Online]. Available: http://www.ezlok.com/TechnicalInfo/MPBrass.html. [Accessed 1 6 2016].

[5] "Aluminum Oxide Al2O3 Material Properties," Accuratus, [Online]. Available: http://accuratus.com/alumox.html. [Accessed 1 6 2016].

[6] B. Jaffe, Piezoelectric Ceramics, Elsevier Science, 2012.

[7] P. G. R. C. M. L. E. J. S. Matthew J. Kundrat, "High performance open loop control of scanning with a small cylindrical cantilever beam," *Journal of Sound and Vibration,* vol. 330, no. 8, pp. 1762-1771, 2011.

[8] Master Bond Inc., "Technical Data Sheet : Master Bond MB Series Cyanoacrylates," [Online]. Available: http://www.masterbond.com/sites/default/files/selector_guides/masterbond_cyanoacrylate.pdf. [Accessed 1 6 2016].

[9] H. a. J. K. a. B. M. Qi, "Durometer hardness and the stress-strain behavior of elastomeric materials," *Rubber Chemistry and Technology,* vol. 76, no. 2, pp. 419-435, 2003.

[10] E. P. Popov, Engineering Mechanics of Solids, Pearson, 1998.

[11] Epoxy Technology, "Tip 19," [Online]. Available: http://www.epotek.com/site/files/Techtips/pdfs/tip19.pdf. [Accessed 6 1 2016].

[12] M. E. a. A. M. G. Lines, Principles and Applications of Ferroelectrics and Related Materials, Oxford : Oxford University Press, 2001.

[13] Z.-R. Q. ,. H.-Y. Y. a. R.-G. X. Hong Zhao, "In situ hydrothermal synthesis of tetrazole coordination polymers with interesting physical properties," *Chemical Society Reviews,* vol. 37, pp. 84-100, 2008.

[14] COMSOL AB, Structural Mechanics Module User's Guide, COMSOL AB, 2015.

[15] COMSOL AB, "Meshing Your Geometry," COMSOL AB, [Online]. Available: https://www.comsol.com/blogs/meshing-your-geometry-various-element-types/. [Accessed 1 6 2016].

[16] Rocscience, "Rocscience," [Online]. Available: https://www.rocscience.com/documents/pdfs/uploads/5836.pdf. [Accessed 4 6 2016].

[17] COMSOL, COMSOL Multiphysics Reference Manual, COMSOL AB, 2015.

[18] CERFACS, "MUMPS," École nationale supérieure d'électronique, d'électrotechnique, d'informatique, d'hydraulique et des télécommunications, [Online]. Available: http://mumps.enseeiht.fr/. [Accessed 5 6 2016].

[19] CTS Electronic Components, "CTS Electronic Components," [Online]. Available: http://venividiwiki.ee.virginia.edu/mediawiki/images/9/95/PZT_5Aand5H.pdf. [Accessed 5 6 2016].

[20] M. H. a. D. L. F. Richardson, "Parameter estimation from frequency response measurements using rational fraction polynomials," in *Proceedings of the 1st international modal analysis conference. Vol. 1*, Union College Schenectady, 1982.

[21] R. P. G. Y. R. J. S. a. H. V. H. Pintelon, "Parametric identification of transfer functions in the frequency domain-a survey," *IEEE transactions on automatic control,* vol. 39, no. 11, pp. 2245-2260, 1994.

[22] S. Z. Z. N. K. W. Shengli Kong, "The size-dependent natural frequency of Bernoulli–Euler micro-beams," *International Journal of Engineering Science,* vol. 46, no. 5, pp. 427-437, 2008.

[23] M. J. Kundrat, "Ph.D Dissertaion on High performance open loop control for fiber scanner imaging and display systems," University of Washington, Seattle, 2010.

[24] M. F. D. N. J. S.Nima Mahmoodi, "On the nonlinear-flexural response of piezoelectrically driven microcantilever sensors," *Sensors and Actuators A: Physical,* vol. 153, no. 2, pp. 171-179, 2009.

[25] D. W. J. a. P. Smith, Nonlinear Ordinary Differential Equations : An Introduction to Dynamical Systems, New York: Oxforf Univeristy Press Inc., 2003.

[26] S. Park, "Analytical modeling of viscoelastic dampers for structural and vibration control," *International Journal of Solids and Structures,* vol. 38, no. 44-45, pp. 8065-8092, 2001.

[27] N. J. S. Nima Mahmoodi, "Non-linear vibrations and frequency response analysis of piezoelectrically driven microcantilevers," *International Journal of Non-Linear Mechanics,* vol. 42, no. 4, pp. 577-587, 2007.

[28] R. P. B. M. C. H. S. E. Yeoh IL, "Electro-Mechanical Modeling and Adaptive Feedforward Control of a Self-Sensing Scanning Fiber Endoscope," *ASME. J. Dyn. Sys., Meas., Control,* 2016.

[29] D. A. Hall, "Review Nonlinearity in piezoelectric ceramics," *Journal of Materials Science,* vol. 36, no. 19, pp. 4575-4601, 2001.

[30] PI-Polytec Group, Micropositioning, NanoPositioning, NanoAutomation (R) Solutions for Cutting-Edge Technologies.

[31] E. J. M. F. J. L. C.-B. Q. Y. S. a. C. M. B. Seibel, "Microfabricated optical fiber with microlens that produces large field-of-view video-rate optical beam scanning for microendoscopy applications," in *Proc. SPIE 4957, Optical Fibers and Sensors for Medical Applications III*, 2003.

Appendix A

MATERIAL PROPERTIES USED IN THE MODEL

Piezo-tube used material properties of the material PZT-5A and the optical fiber used material properties of the material Silica glass from the COMSOL Material Library. Material properties of the rest of the domains are given below.

Table 2: Material properties of the Ceramic Collar

Young's Modulus	300×10^9 Pa
Poisson's ratio	0.21
Density	3720

Table 3: Material properties of the cyanoacrylate (CA) joints

Young's Modulus	2.6738×10^9 Pa
Poisson's ratio	0.358
Density	1112.48

Table 4: Material properties of the Brass holder

Young's Modulus	97×10^9 Pa
Poisson's ratio	0.31
Density	8490